Mammalian Polycomb-mediated repression of *Hox* genes requires the essential spliceosomal protein Sf3b1

Kyoichi Isono,[1] Yoko Mizutani-Koseki,[1] Toshihisa Komori,[2] Marion S. Schmidt-Zachmann,[3] and Haruhiko Koseki[1,4]

[1]Developmental Genetics Group, RIKEN Research Center for Allergy and Immunology, Tsurumi-ku, Yokohama 230-0045, Japan; [2]Department of Medicine III, Osaka University Medical School, Suita, Osaka 565-0871, Japan; [3]Division of Cell Biology, German Cancer Research Center, D-69120 Heidelberg, Germany

Polycomb group (PcG) proteins are responsible for the stable repression of homeotic (*Hox*) genes by forming multimeric protein complexes. We show (1) physical interaction between components of the U2 small nuclear ribonucleoprotein particle (U2 snRNP), including Sf3b1 and PcG proteins Zfp144 and Rnf2; and (2) that *Sf3b1*-heterozygous mice exhibit skeletal transformations concomitant with ectopic *Hox* expressions. These alterations are enhanced by *Zfp144* mutation but repressed by *Mll* mutation (a trithorax-group gene). Importantly, the levels of Sf3b1 in PcG complexes were decreased in *Sf3b1*-heterozygous embryos. These findings suggest that Sf3b1–PcG protein interaction is essential for true PcG-mediated repression of *Hox* genes.

Supplemental material is available at http://www.genesdev.org.

Received November 29, 2004; revised version accepted January 14, 2005.

During mammalian development, spatially and quantitatively appropriate homeotic (*Hox*) gene expression is essential for the anterior–posterior specification of axial structures (McGinnis and Krumlauf 1992; Duboule and Morata 1994). The maintenance of the *Hox* gene expres-

1999; Francis and Kingston 2001; Simon and Tamkun 2002; Orlando 2003). In general, PcG proteins act as repressors to maintain the silent state, while the trxG proteins are activators that maintain *Hox* gene transcription. PcG proteins constitute large, chromatin-associated multiprotein complexes, which in mammals can be classified into at least two different classes. The Class I complex, which contains Eed/Ezh2, is associated with histone deacetylase and methyltransferase activity. The PRC1 or Class II complex consists of, for example, Zfp144 (Mel18), Rnf2 (Ring1B), Cbx2/M33, and Phc2/Edr2. The Class II complex, which characteristically includes the products from highly related pairs of genes, has been shown to inhibit nucleosome remodeling by the SWI/SNF complex in vitro (Shao et al. 1999). However, as the inhibition requires preincubation of the Class II with the nucleosomal template (it does not occur when Class II and SWI/SNF products are added together), this suggests that the Class II complex does not interact directly with SWI/SNF, but instead competes for the nucleosome template. Possibly, it is this binding of the Class II complex, which prevents nucleosome remodeling, that silences the genes by blocking the access of transcription activators to *cis*-regulatory elements such as promoters and enhancers (Francis et al. 2001). Interestingly, recent studies have proposed an alternative mechanism for maintaining gene silence (Breiling et al. 2001; Saurin et al. 2001). Fly Class II complex includes general transcription factors such as TBP and TBP-associated proteins at promoter regions. Using an in vitro assay, King et al. (2002) showed that the fly complex was able to inhibit transcription by RNA polymerase II at particular steps even after activator binding. This raises the possibility that the Class II complex might act directly on the functioning of the transcriptional machinery. However, whether this silencing mechanism is active at *Hox* loci during mammalian embryo development is not clear. In order to achieve a better understanding of the molecular basis of PcG complex-mediated repressions, we believe that it is important to identify PcG complex-associated non-PcG proteins and subsequently investigate the genetic impact of such proteins on PcG complexes. In this paper, we identified an essential spliceosomal protein Sf3b1 that physically interacts with the Class II PcG proteins and generated *Sf3b1* knockout mice. Surprisingly, *Sf3b1*$^{+/-}$ mice exhibited skeletal phenotypes that are usually observed with *PcG* mutation. Furthermore, genetic interactions between *Sf3b1* and *Zfp144* or the trxG gene *Mll* mutations were also shown. Therefore, it appears that Sf3b1 and the Class II PcG proteins are functionally interacting on the *Hox* loci in developing embryos.

Two partial cDNA clones encoding amino acid 1–489 and 312–777 regions of mouse spliceosomal protein Sf3b1 have been isolated as interactors for the mammalian PcG proteins Zfp144 and Rnf2, respectively, by yeast two-hybrid screening (Fig. 1A). Physical interactions between Sf3b1 and PcG proteins were first examined by glutathione S-transferase (GST) pull-down assay. Nuclear proteins were extracted from mouse embryonic stem (ES) cells and subsequently precipitated by GST–Rnf2 and GST–Zfp144 fusion proteins. The precipitates were subjected to immunoblotting with anti-Sf3b1 antibody. Endogenous Sf3b1 was clearly coprecipitated with GST–Rnf2 and GST–Zfp144 (Fig. 1B). Moreover, assay with Rnf2 truncates revealed that Sf3b1 specifically in-

[*Keywords*: *Hox* genes; Polycomb group; knockout mice; spliceosomal proteins]
[4]Corresponding author.
E-MAIL koseki@rcai.riken.jp; FAX 81-45-503-9690.
Article and publication are at http://www.genesdev.org/cgi/doi/10.1101/gad.1284605.

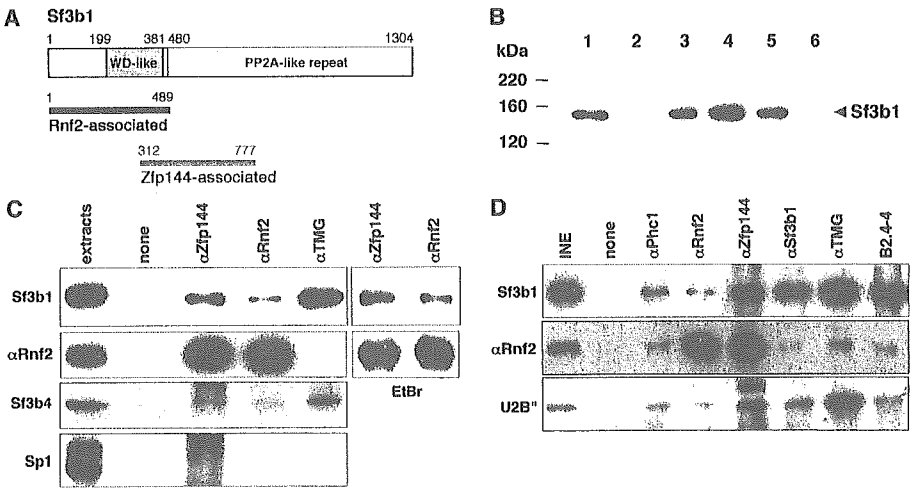

Figure 1. Physical interaction between Sf3b1 and PcG proteins. (*A*) Primary structure of Sf3b1 (Isono et al. 2001). Sf3b1 has WD-40 like repeats and PP2A repeats (usually termed HEAT motifs) originally identified in the PR65 subunit of protein phosphatase 2A. The N-terminal region (amino acids 1–489) and the internal region (amino acids 312–777), respectively, were associated with Rnf2 and Zfp144 in the yeast two-hybrid system. (*B*) GST pull-down assays probed with the Sf3b1-specific antibody. Nuclear extracts from ES cells were incubated with GST alone (lane 2) and GST fusions with Zfp144 (lane 3), Rnf2 (lane 4), and the N-terminal (lane 5) or C-terminal (lane 6) regions of Rnf2. In lane 1, one-fifteenth volume of extract sample used in a reaction was applied. (*C*) Coimmunoprecipitation with whole-cell lysates. Lysate of a mouse embryo at 10.75–11.25 dpc was incubated with or without antibodies to Zfp144, Rnf2, or TMG. Each precipitant was divided into two, and each was used in immunoblotting with Sf3b1 and Rnf2 or Sp1 and Sf3b4 antibodies. Anti-Sp1 was used as a negative control. In each "extract" lane, one-fortieth volume of extract sample used in a reaction was applied. In addition, lysates treated with ethidium bromide (EtBr) were also used to exclude DNA. (*D*) Coimmunoprecipitation with chromatin-rich lysates. Insoluble nuclear extract from an embryo at 10.75–11.25 dpc was prepared by osmotic shock, solubilized by sonication, and then incubated with antibodies. Phc1 is a mouse homolog to the fly PcG protein, Polyhomeotic (the fly protein homologous to mouse Phc1). B2.4-4 is a polyclonal antibody against the *Xenopus* Sf3b1, which has an epitope different from the monoclonal antibody (αSf3b1). In the "INE" lane, one-fortieth volume of the insoluble extract used in a reaction was applied.

teracts with the N-terminal region (amino acids 1–188) but not with the C-terminal region (amino acids 189–336). Thus, Sf3b1 probably has the potential to bind directly to Rnf2 and Zfp144.

We examined the in vivo interaction further in whole-cell extracts from 11.5 d post-coitus (dpc) embryos in which PcG complexes have been shown to act as repressors of *Hox* gene expression (Fig. 1C; Akasaka et al. 1996). A significant, but substoichiometric amount, of Sf3b1 was reproducibly coimmunoprecipitated with Zfp144 and Rnf2, as revealed by comparison with anti-Rnf2 immunoblotting. The presence of ethidium bromide did not affect these Sf3b1–Zfp144/Rnf2 interactions, which suggests that they were DNA independent. As Sf3b1 is known to be a component of U2 snRNP (Krämer 1996; Schmidt-Zachmann et al. 1998), we therefore examined other U2 snRNP components, Sf3b4 (SAP49), U2B", and U snRNAs. In the conventional nuclear extracts, Sf3b4 was also coprecipitated with PcG proteins while anti-2,2,7-trimethylguanosine (TMG) antibody, which reacts to the 5′ cap of U snRNAs characteristic for the U1, U2, U5, and U4/U6 snRNPs (Krämer 1996), failed to coprecipitate Rnf2. It is, however, possible that excess nucleoplasmic spliceosomal proteins or nucleoplasmic interaction between monomeric Sf3b1 and the PcG proteins would obscure experimental outcomes. To exclude these possibilities, we employed nuclear insoluble fraction extracted under high salt condition, in which proteins closely associated to chromatin are presumed to be concentrated. The fractions were solubilized by sonication and used in immunoprecipitation. Coimmunoprecipitation of Rnf2 with Phc1/Rae28 and Zfp144 indicated the presence of PcG multimeric complexes in this fraction. Sf3b1 and U2B" were coimmunoprecipitated with Phc1, Rnf2, and Zfp144. Concordantly, two different anti-Sf3b1 antibodies were able to coimmunoprecipitate Rnf2, reinforcing the interaction between Sf3b1 and PcG proteins. Notably, significant amounts of Rnf2 as well as Sf3b1 and U2B" were coimmunoprecipitated by anti-TMG antibody, implying the association of the U2 snRNA to PcG complexes. Importantly, these U2 snRNP components bound to the PcG proteins were detected in similar proportions (Fig. 1C,D). Taken together, these results show that it is likely that PcG complexes associate with at least part of the U2 snRNP rather than Sf3b1 alone.

To examine the biological implications of *Sf3b1*, we have generated an *Sf3b1*-mutant allele by replacing four exons with the *neo* gene in the opposite direction. *Sf3b1* null homozygotes died during preimplantation development around the 16- to 32-cell stage. Heterozygotes were externally normal and healthy, although the levels of *Sf3b1* mRNA and Sf3b1 were significantly reduced (Supplementary Fig. S1). Since *PcG* mutants exhibit posterior transformations of the vertebrae (Akasaka et al. 1996; Gould 1997; Suzuki et al. 2002), we examined axial skeletal preparations of $Sf3b1^{+/-}$ newborn pups backcrossed five times (N5) to C57BL/6 background. Significantly, $Sf3b1^{+/-}$ mice exhibited various skeletal alterations along the anterior–posterior axis (Table 1). In the cervical region of $Sf3b1^{+/-}$ mutants, the seventh cervical vertebra (C7) had incomplete ectopic ribs, either unilaterally or bilaterally fused with the first thoracic rib (27%), indicating transformations of C7 toward the first thoracic vertebra (T1) (Fig. 2B). Twenty-nine percent of $Sf3b1^{+/-}$ mutants had a prominent spinous process, characteristic for the second thoracic vertebra (T2), incorrectly associated with T1 (Fig. 2C), suggesting a T1 → T2

Table 1. *Summary of skeletal transformations in mutant mice*

Parents	B6 × *Sf3b1*$^{+/-}$ (N4)		*Mel18*$^{+/-}$ × *Sf3b1*$^{+/-}$ (N4)				*Mll*$^{+/-}$ × *Sf3b1*$^{+/-}$ (N6)			
Transformation types	wt (n = 50)	*Sf3b1*$^{+/-}$ (n = 48)	wt (n = 21)	*Mel18*$^{+/-}$ (n = 18)	*Sf3b1*$^{+/-}$ (n = 22)	*Mel18*$^{+/-}$*Sf3b1*$^{+/-}$ (n = 20)	wt (n = 14)	*Mll*$^{+/-}$ (n = 23)	*Sf3b1*$^{+/-}$ (n = 25)	*Mll*$^{+/-}$*Sf3b1*$^{+/-}$ (n = 15)
C7 → T1	0 (0)	27 (13)	0 (0)	6 (1)	32 (7)	45 (9), [a]4/9	0 (0)	0 (0)	68 (17)	0 (0)
T1 → T2	0 (0)	29 (14)	0 (0)	11 (2)	23 (5)	75 (15)	7 (1)	0 (0)	60 (15)	0 (0)
T13 → L1	0 (0)	6 (3)	0 (0)	28 (5)	14 (3)	50 (10)	0 (0)	9 (2)	8 (2)	13 (2)
L6 → S1	22 (11)	88 (42)	62 (13)	89 (16)	100 (22)	100 (20)	21 (3)	61 (14)	88 (22)	87 (13)

[a]Four out of nine C7 → T1 mice exhibited complete first ribs associated with the C7 vertebra (see Fig. 2G).
Unit: % (n).

transformation. In addition, *Sf3b1*$^{+/-}$ mice had only 12 ribs (6%) (Fig. 2F) and five lumbar vertebrae (88%) (Fig. 2E–F), indicating T13 → L1 and L6 → S1 transformations, respectively. Thus, *Sf3b1*$^{+/-}$ mice exhibit skeletal phenotypes similar to *PcG* mutants although the penetrance is rather low. We investigated next whether these skeletal alterations, seen with *Sf3b1*$^{+/-}$, were associated with anterior shifts of *Hox* gene expression boundaries as well as *PcG* mutants (Akasaka et al. 1996). The *Hoxb8* expression was extended to the seventh prevertebrae in three out of five *Sf3b1*$^{+/-}$ embryos and from the eighth prevertebra in wild type (Fig. 2L–N), and also *Hoxb6* and *Hoxc6* were ectopically expressed in the sixth prevertebrae in *Sf3b1*$^{+/-}$ embryos (Fig. 2I–K,O–Q). Significant changes were not observed for *Hoxa5*, *Hoxb3*, *Hoxb4*, or *Hoxd4* expression in the paraxial me-

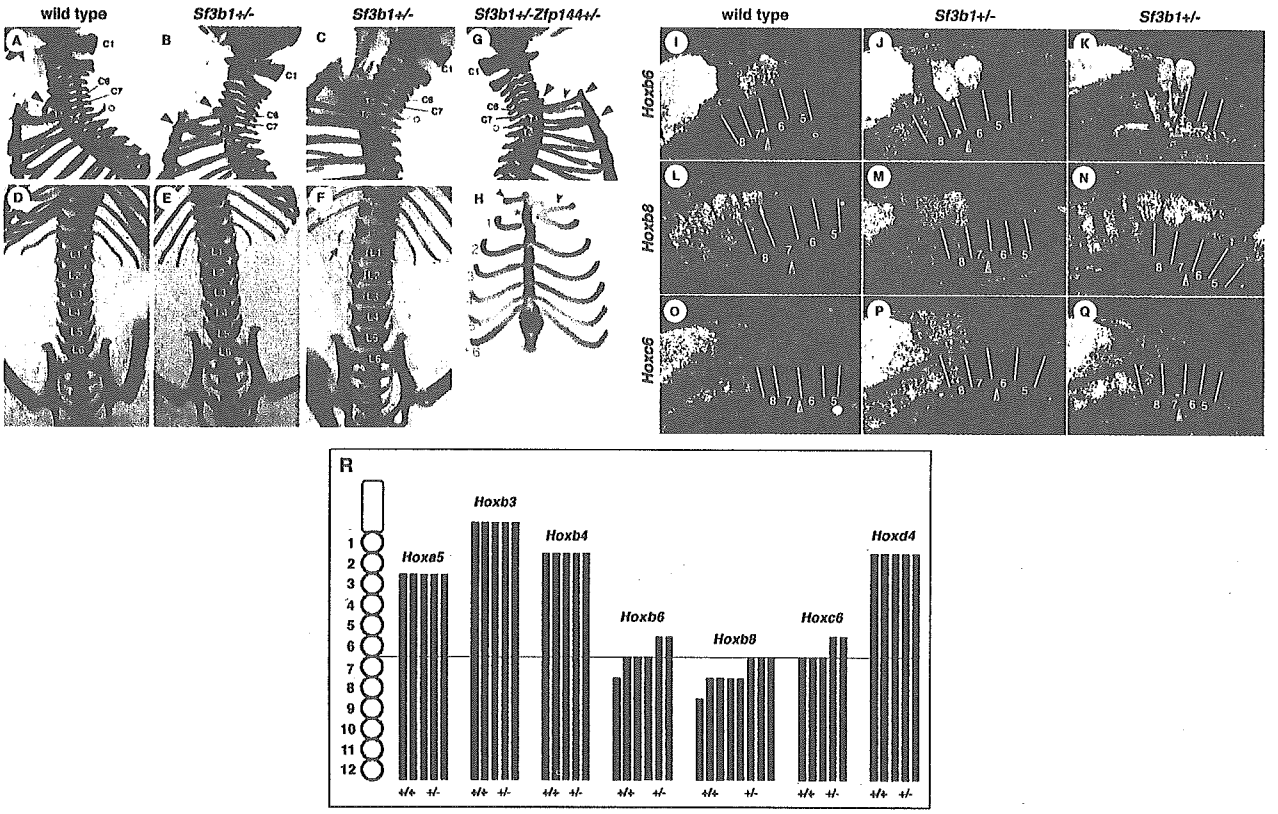

Figure 2. Skeletal abnormalities and ectopic *Hox* expressions in *Sf3b1*$^{+/-}$ mice. Cervical–thoracic (lateral view) and thoracic–sacral (ventral view) regions of wild-type (*A,D*) and two independent *Sf3b1*$^{+/-}$ (*B,C,E,F*) newborns are shown. Numbering of vertebrae of mutants makes them consistent with those of wild type. In wild type, C6 and T2 vertebrae have characteristic ventral processes as indicated by arrowheads (orange) and a prominent spinous process (yellow circle), respectively. An arrow indicates the disappearance of the T13 rib in the *Sf3b1*$^{+/-}$ mutant. (*G,H*) the lateral view of cervical–thoracic region and the ventral view of rib cage of the *Sf3b1*$^{+/-}$*Zfp144*$^{+/-}$ compound mutant. Ectopic ribs with C7 are represented by black arrowheads. An asterisk indicates an additional ossification center. Ribs numbered as 1–6 associate with T1–T6 vertebrae, respectively. The right ectopic rib with C7 separates from the rib with T1 on the sternum, as shown by green arrowheads. (*I–Q*) RNA in situ hybridization of *Hox* genes in embryos at 11.5 dpc. Boundaries of prevertebrae in lateral view are indicated by lines and the prevertebrae are numbered from prospective C1. Vertebral arteries are indicated by arrowheads and anterior boundaries of expressions are indicated by arrows. In *Sf3b1*$^{+/-}$ embryos, anterior boundaries of *Hoxb6*, *Hoxb8*, and *Hoxc6* expressions are shown to shift by sixth, seventh, and sixth prevertebrae, respectively. (*R*) Summary of *Hoxa5*, *Hoxb3*, *Hoxb4*, *Hoxb6*, *Hoxb8*, *Hoxc6*, and *Hoxd4* expressions in the paraxial mesoderm is depicted schematically. Each black (wild type) or gray (*Sf3b1*$^{+/-}$) bar represents expressional regions and a number of bars show individual embryos. Segment numbers are counted from the prospective C1.

soderm of *Sf3b1*$^{+/-}$ embryos (Fig. 2R). However, we found a subtle alteration of the *Hoxd4* expression in the second branchial arch of *Sf3b1*$^{+/-}$ embryos (data not shown). In summary, the expressions of several *Hox* genes were anteriorly extended in the paraxial mesoderm and second branchial arch in *Sf3b1*$^{+/-}$ embryos. These observations are consistent with the axial skeletal alterations observed in *Sf3b1*$^{+/-}$ mice. Therefore, we concluded that Sf3b1 mediates the repression of *Hox* genes.

Individual *PcG* mutations have been shown to mutually enhance their phenotypes (Bel et al. 1998; Akasaka et al. 2001; Suzuki et al. 2002). To investigate whether this Sf3b1-mediated repression involves PcG complexes, we examined the genetic interactions between *Zfp144* and *Sf3b1* mutations. In *Sf3b1*$^{+/-}$*Zfp144*$^{+/-}$ double heterozygotes, the formation of an additional ossification center in the sternum, and the detachment of the ribs of T7 from the sternum, represented an anterior shift of the sternum of one segment width (Fig. 2H). The ectopic ribs associated with C7 mimicked perfect ribs and formed joints with the anteriorly shifted sternum (Fig. 2G). These alterations were observed in four (44%) out of nine double mutants that displayed perfect C7 → T1 transformation but were not observed in either of the single mutants (Table 1). In addition to the ectopic ribs, the frequencies of other transformations were much higher in the double mutants. In particular, the T1 → T2 transformation occurred at a much higher penetrance: 75% in double mutants versus only 11% or 23% in either single mutant, suggesting that the single phenotypes of respective mutations were enhanced in the presence of each other. We further examined the impact of the *Sf3b1* mutation on the mutation at the *mixed lineage leukemia* (*Mll*) gene (Yu et al. 1995), a mammalian homolog of the *trithorax* gene of *Drosophila melanogaster*, whose product is antagonistic to *PcG* mutations (Hanson et al. 1999). Posterior transformations at the cervico–thoracic transitional zone caused by *Sf3b1* mutation were completely restored by *Mll* mutation (Table 1; Yagi et al. 1998). Therefore, it is likely that Sf3b1 has an antagonistic relationship to trxG proteins as well as PcG complexes. Taken together, these results indicate that Sf3b1 is functionally involved in PcG repressive complexes.

Since Sf3b1 is involved essentially in pre-mRNA splicing, the basal expression levels of genes, including *PcG* or *Hox* genes, may be profoundly altered in *Sf3b1*$^{+/-}$ mice, leading to homeotic transformations. To investigate this, a basal activity of splicing was examined with nuclear extracts from 10.5 dpc *Sf3b1*$^{+/-}$ embryos in which the Sf3b1 level was reduced up to ~75% but Rnf2 accumulated at normal level (data not shown). Despite such lower quantities of Sf3b1, their splicing activity was equal because of the same ratio of their spliced forms (Fig. 3A). Furthermore, while expression levels of *Sf3b1* were reduced by half in *Sf3b1*$^{+/-}$ embryos, those of five PcG genes, *Zfp144*, *Rnf2*, *Eed*, *Cbx2/M33*, and *Phc2/Edr2*; three *Hox* genes, *Hoxb3*, *Hoxb6*, and *Hoxb8*; and a metabolic gene, *Hprt*, were not (Fig. 3B). Thus, homeotic transformations in *Sf3b1*$^{+/-}$ mice appear to be independent of the alteration of general gene expression. Next, we investigated the amount of Sf3b1 associated with PcG proteins in *Sf3b1*$^{+/-}$ embryos. While Zfp144- or Rnf2-associated Sf3b1 were clearly decreased in *Sf3b1*$^{+/-}$ embryos, Rnf2 was precipitated equally in both embryos (Fig. 3C). It was also notable

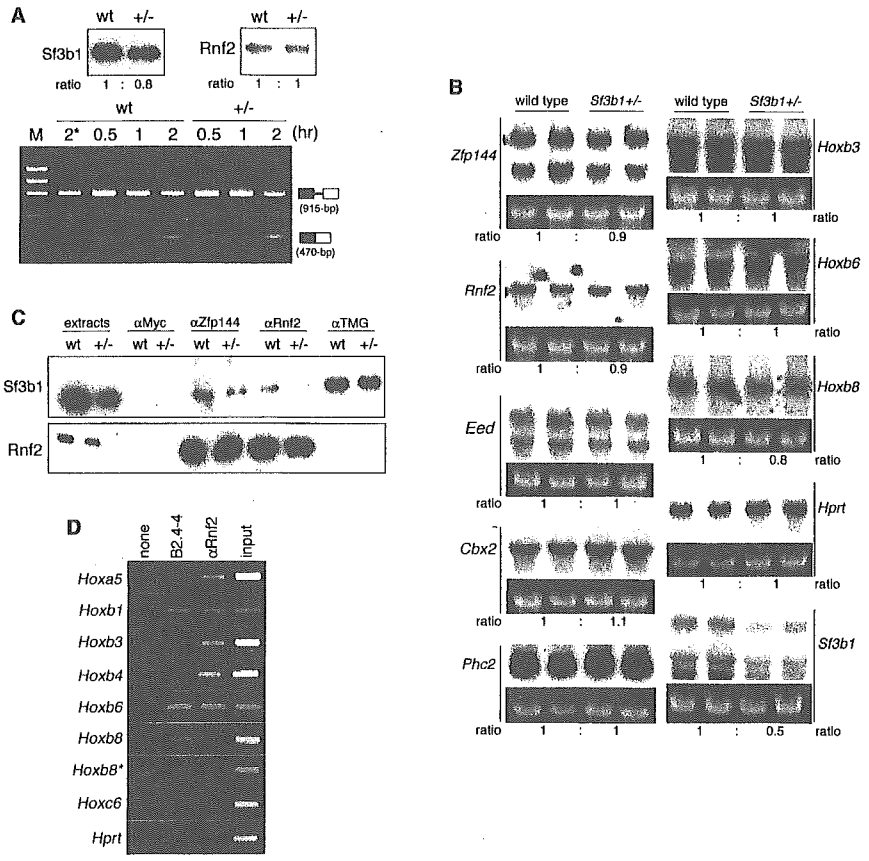

Figure 3. Comparison of wild-type and *Sf3b1*$^{+/-}$ embryos. Genotyping of embryos was performed with total DNA from yolk sacs. (*A*) In vitro splicing assay. The soluble fraction of a nuclear extract was prepared from wild-type or *Sf3b1*$^{+/-}$ embryos at 10.5 dpc. Equal amounts (60 μg) of total protein were confirmed by Western blotting with anti-Sf3b1 and anti-Rnf2 antibodies (*upper* panels) and subjected to a splicing assay (*lower* panel). One-step RT–PCR revealed that unspliced forms consisting of two exons and an intron (upper bands) as the RNA substrates were converted into spliced forms (lower bands) by the splicing reaction. Band intensities were measured by the image-processing program Image J and the ratios of *Sf3b1*$^{+/-}$ to wild type were obtained.(*B*) Northern analysis of total RNAs (15 μg each) from independent embryos at 12.5 dpc. Ethidium-bromide-stained 28S rRNAs prior to transfer to membranes are displayed *below* their blots. Intensity of each detected band was normalized by their rRNAs and then the ratios of *Sf3b1*$^{+/-}$ to wild type were calculated (indicated *below* their panels). (*C*) Immunoprecipitation assay with embryos at 11.5 dpc. Three independent embryos with the same genotype were sonicated individually, and the soluble lysates were mixed and then divided into four. Each was immunoprecipitated with a specific antibody. (*D*) ChIP assay with ES cells. Cross-linked chromatins were immunoprecipitated with or without indicated antibodies and subjected to amplification of *Hox* and *Hprt* regions (260–480 bp) by PCR. The amplified regions were detected in 1.5% agarose gels.

that the anti-TMG precipitates contained almost equal levels of Sf3b1, suggesting that the majority of U2 snRNP were not significantly altered in *Sf3b1*$^{+/-}$ embryos. This finding agrees well with the normal expression of other genes described above. Therefore, the heterozygous loss of *Sf3b1* gene results in significant reduction of Sf3b1 associated with PcG complexes, strongly suggesting a repressive mechanism of *Hox* genes via interaction with PcG complexes.

We finally examined whether Sf3b1 is closely associated to *Hox* genomic regions together with PcG proteins by chromatin immunoprecipitation (ChIP) assay. Various *Hox* cluster genes, including *Hoxa5*, *Hoxb1*, *Hoxb3*, *Hoxb4*, *Hoxb6*, *Hoxb8*, *Hoxb9*, and *Hoxc6*, were depressed in *Rnf2*$^{-/-}$ ES cells, indicating the involvement of PcG proteins in regulation of *Hox* expressions in ES cells (de Napoles et al. 2004; K. Isono and H. Koseki, unpubl.). Accordingly, we found obvious immunoprecipitation of 5′ genomic regions (260–480 bp) of *Hoxa5*, *Hoxb1*, *Hoxb3*, *Hoxb4*, *Hoxb6*, *Hoxb8*, and *Hoxc6* in wild-type ES cells by anti-Rnf2 antibody but not *Hprt* gene, which is not derepressed in *Rnf2*$^{-/-}$ ES cells (Fig. 3D). Likewise, we found association of Zfp144 to these *Hox* genes (K. Isono and H. Koseki, unpubl.). Anti-Sf3b1 antibody also precipitated a significant amount of 5′ genomic regions of these *Hox* genes while either anti-Rnf2 or anti-Sf3b1 antibody failed to precipitate the second exonic region of *Hoxb8* gene (indicated by *Hoxb8** in Fig. 3D). These findings indicate that the Sf3b1 and PcG proteins colocalize locally on the 5′ regions of individual *Hox* genes. It is also noteworthy that the relative degree of Sf3b1 association in comparison with the Rnf2 is greater at the *Hoxb6*, *Hoxb8*, and *Hoxc6* genomic regions than the *Hoxa5*, *Hoxb3*, and *Hoxb4* genes. This is in good agreement with another observation in *Sf3b1*$^{+/-}$ embryos that the expression of *Hoxb6*, *Hoxb8*, and *Hoxc6* was derepressed but not the *Hoxa5*, *Hoxb3*, or *Hoxb4* (summarized in Fig. 2R). Taken together, these results show that it is likely that a mechanistic link between Sf3b1 and PcG complexes regulates *Hox* gene expression via direct binding to *Hox* genomic regions.

Our results show a significant and novel mechanistic link between Sf3b1 (together probably with other U2 snRNP components) and PcG repressive complexes on *Hox* loci. This idea is strongly supported by our recent observation that heterozygous mutant mice for *Sf3b2*, another U2 snRNP component, exhibited skeletal abnormality similar to *Sf3b1* phenotypes: 10 out of 14 targeting mice (71%) had L6 to S1 transformation compared with two out of 18 wild-type mice (11%) (K. Isono and H. Koseki, unpubl.). However, although with respect to the PcG-mediated repression in the transcriptional-competent regions, our findings are in general accord with previous reports (Breiling et al. 2001; Saurin et al. 2001; King et al. 2002; Cmarko et al. 2003; de Graaff et al. 2003; Dellino et al. 2004), nevertheless they indicate the presence a different gene silencing mechanism. Evidence that the level of Sf3b1 in PcG complexes affects the expressional boundary of *Hox* genes implies that Sf3b1 supports the activity of PcG complexes. The simplest explanation is that Sf3b1/U2 snRNP might be a PcG protein and could form repressive PcG complexes together with other PcG proteins. A more interesting hypothesis is that this interaction constitutes part of a mechanism that is designed to maintain the amount of *Hox* transcripts required to confer the appropriate positional identities. Regulation of *Hox* expressions in the vicinity of their boundaries is thought to be loose, because even wild type occasionally exhibits homeotic transformations (Table 1 and Akasaka et al. 1996). RNAs, mistranscribed beyond loose repression, may be tethered by Sf3b1/U2 snRNP bound to PcG complex, leading to the arrest of splicing and a normal *Hox* boundary as a consequence. However, in *Sf3b1*$^{+/-}$ cells, because of the decrease of PcG complex-bound Sf3b1, such mistranscribed RNAs become easily associated with splicing-active nucleoplasmic Sf3b1/U2 snRNP. This association leads to the achievement of a splicing reaction, which results in the anterior shift of *Hox* expression. In support of this model is the important evidence that the *Mll* mutation completely suppressed *Sf3b1* phenotypes, indicating that the PcG-like function of Sf3b1 is very susceptible to levels of Mll; in other words the acting points of both proteins are spatially very close. Of further note is the fact that the human MLL supercomplex includes the 116-kDa protein specific to the U5 snRNP, which acts on pre-mRNA following the U2 snRNP (Nakamura et al. 2002). Finally, it appears that there are multiple interacting surfaces between PcG complexes and gene expression machineries. It might be that, through this interaction, PcG complexes act as a part of the modules that sense the transcriptional status in transcriptional-competent regions of the *Hox* cluster.

Materials and methods

Yeast two-hybrid screening, immunoprecipitation and GST pull-down assays, ChIP analysis, in vitro splicing assay, and knockout mice are described in the Supplemental Material.

Acknowledgments

We thank Drs. Miguel Vidal and Tsukasa Oda for providing *Rnf2* cDNA and pBTM116, respectively. In addition, we thank Drs. Takeshi Akasaka and Tomomi Kaneko, Ms. Kazumi Nemoto, Minako Ogawa, Misao Uchida, and Sanae Takeda for help with this work, and Drs. Achim Gossler and Miguel Vidal for their critical reading of the manuscript. This study was supported by Special Coordination Funds for Promoting Science and Technology from the Ministry of Education, Culture, Sports, Science and Technology, the Japanese Government.

References

Akasaka, T., Kanno, M., Balling, R., Mieza, M.A., Taniguchi, M., and Koseki, H. 1996. A role for *Mel18*, a *Polycomb* group-related vertebrate gene, during the anteroposterior specification of the axial skeleton. *Development* **122:** 1513–1522.

Akasaka, T., van Lohuizen, M., van der Lugt, N., Mizutani-Koseki, Y., Kanno, M., Taniguchi, M., Vidal, M., Alkema, M., Berns, A., and Koseki, H. 2001. Mice doubly deficient for the Polycomb Group genes *Mel18* and *Bmi1* reveal synergy and requirement for maintenance but not initiation of *Hox* gene expression. *Development* **128:** 1587–1597.

Bel, S., Core, N., Djabali, M., Kieboom, K., van der Lugt, N., Alkema, M.J., and van Lohuizen, M. 1998. Genetic interactions and dosage effects of Polycomb group genes in mice. *Development* **125:** 3543–3551.

Breiling, A., Turner, B. M., Bianchi, M. E., and Orlando, V. 2001. General transcription factors bind promoters repressed by Polycomb group proteins. *Nature* **412:** 651–655.

Cmarko, D., Verschure, P.J., Otte, A.P., van Driel, R., and Fakan, S. 2003. Polycomb group gene silencing proteins are concentrated in the perichromatin compartment of the mammalian nucleus. *J. Cell Sci.* **116:** 335–343.

de Graaff, W., Tomotsune, D., Oosterveen, T., Takihara, Y., Koseki, H., and Deschamps, J. 2003. Randomly inserted and targeted Hox/reporter fusions transcriptionally silenced in Polycomb mutants. *Proc. Natl. Acad. Sci.* **100:** 13362–13367.

Dellino, G.I., Schwartz, Y.B., Farkas, G., McCabe, D., Elgin, S.C.R., and Pirrotta, V. 2004. Polycomb silencing blocks transcription initiation. *Mol. Cell* **13:** 887–893.

de Napoles, M., Mermoud, J.E., Wakao, R., Tang, Y.A., Endoh, M., Appanah, R., Nesterova, T.B., Silva, J., Otte, A.P., Vidal, M., et al. 2004. Polycomb group proteins Ring1A/B link ubiquitylation of histone H2A to heritable gene silencing and X inactivation. *Dev. Cell* **7:** 663–676.

Duboule, D. and Morata, G. 1994. Colinearity and functional hierarchy among genes of the homeotic complexes. *Trends Genet.* **10:** 358–364.

Francis, N.J. and Kingston, R.E. 2001. Mechanisms of transcriptional memory. *Nat. Rev. Mol. Cell Biol.* **2:** 409–421.

Francis, N.J., Saurin, A.J., Shao, Z., and Kingston, R.E. 2001. Reconstitution of a functional core Polycomb repressive complex. *Mol. Cell* **8:** 545–556.

Gould, A. 1997. Functions of mammalian Polycomb group and trithorax group related genes. *Curr. Opin. Genet. Dev.* **7:** 488–494.

Hanson, R.D., Hess, J.L., Yu, B.D., Ernst, P., van Lohuizen, M., Berns, A., van der Lugt, M.N.T., Shashikant, C.S., Ruddle, F.H., Seto, M., et al. 1999. Mammalian *Trithorax* and *Polycomb*-group homologues are antagonistic regulators of homeotic development. *Proc. Natl. Acad. Sci.* **96:** 14372–14377.

Isono, K., Abe, K., Tomaru, Y., Okazaki, Y., Hayashizaki, Y., and Koseki, H. 2001. Molecular cloning, genetic mapping, and expression of the mouse Sf3b1 (SAP155) gene for the U2 snRNP component of spliceosome. *Mamm. Genome* **12:** 192–198.

King, I.F.G., Francis, N.J., and Kingston, R.E. 2002. Native and recombinant Polycomb group complexes establish a selective block to template accessibility to repress transcription in vitro. *Mol. Cell. Biol.* **22:** 7919–7928.

Krämer, A. 1996. The structure and function of proteins involved in mammalian pre-mRNA splicing. *Annu. Rev. Biochem.* **65:** 367–409.

McGinnis, W. and Krumlauf, R. 1992. Homeobox genes and axial patterning. *Cell* **68:** 283–302.

Nakamura, T., Mori, T., Tada, S., Krajewski, W., Rozovskaia, T., Wassell, R., Dubois, G., Mazo, A., Croce, C.M., and Canaani, E. 2002. ALL-1 is a histone methyltransferase that assembles a supercomplex of proteins involved in transcriptional regulation. *Mol. Cell* **10:** 1119–1128.

Orlando, V. 2003. Polycomb, epigenomes, and control of cell identity. *Cell* **112:** 599–606.

Satijn, D.P.E. and Otte, A.P. 1999. Polycomb group protein complexes: Do different complexes regulate distinct target genes? *Biochim. Biophys. Acta* **1447:** 1–16.

Saurin, A.J., Shao Z., Erdjument-Bromage, H., Tempst, P., and Kingston R.E. 2001. A *Drosophila* Polycomb group complex includes Zeste and dTAFII proteins. *Nature* **412:** 655–660.

Schmidt-Zachmann, M.S., Knecht, S., and Krämer, A. 1998. Molecular characterization of a novel, widespread nuclear protein that colocalizes with spliceosome components. *Mol. Biol. Cell* **9:** 143–160.

Shao, Z. Raible, F., Mollaaghababa, R., Guyon, J.R., Wu, C.-T., Bender, W., and Kingston, R.E. 1999. Stabilization of chromatin structure by PRC1, a Polycomb complex. *Cell* **98:** 37–46.

Simon J.A. and Tamkun, J.W. 2002. Programming off and on states in chromatin: Mechanisms of Polycomb and trithorax group complexes. *Curr. Opin. Genet. Dev.* **12:** 210–218.

Suzuki, M., Mizutani-Koseki, Y., Fujimura, Y., Miyagishima, H., Kaneko, T., Takada, Y., Akasaka, T., Tanzawa, H., Takihara, Y., Nakano, M., et al. 2002. Involvement of the Polycomb-group gene Ring1B in the specification of the anterior–posterior axis in mice. *Development* **129:** 4171–4183.

Yagi, H., Deguchi, K., Aono, A., Tani, Y., Kishimoto, T., and Komori, T. 1998. Growth disturbance in fetal liver hematopoiesis of MLL-mutant mice. *Blood* **92:** 108–117.

Yu, B.D., Hess, J.L., Horning, S.E., Brown, G.A., and Korsmeyer, S.J. 1995. Altered Hox expression and segmental identity in Mll-mutant mice. *Nature* **378:** 505–508.

THE JOURNAL OF BIOLOGICAL CHEMISTRY
Vol. 280, No. 16, Issue of April 22, pp. 16417–16426, 2005
Printed in U.S.A.
© 2005 by The American Society for Biochemistry and Molecular Biology, Inc.

Estrogen, Insulin, and Dietary Signals Cooperatively Regulate Longevity Signals to Enhance Resistance to Oxidative Stress in Mice*

Received for publication, January 25, 2005, and in revised form, February 15, 2005
Published, JBC Papers in Press, February 15, 2005, DOI 10.1074/jbc.M500924200

Tomonori Baba‡§, Takahiko Shimizu‡, Yo-ichi Suzuki‡, Midori Ogawara‡, Kyo-ichi Isono¶‖, Haruhiko Koseki¶‖, Hisashi Kurosawa§, and Takuji Shirasawa‡**

From the ‡Department of Molecular Gerontology, Tokyo Metropolitan Institute of Gerontology, Itabashi-ku, Tokyo, 173-0015, Japan, ¶Molecular Embryology, Graduate School of Medicine, Chiba University, Chiba, 260-8670, Japan, and §Department of Orthopedics, Juntendo University, Bunkyo-ku, Tokyo, 113-8421, Japan

To investigate the biological significance of a longevity mutation found in *daf-2* of *Caenorhabditis elegans*, we generated a homologous murine model by replacing Pro-1195 of insulin receptors with Leu using a targeted knock-in strategy. Homozygous mice died in the neonatal stage from diabetic ketoacidosis, whereas heterozygous mice showed the suppressed kinase activity of the insulin receptor but grew normally without spontaneously developing diabetes during adulthood. We examined heterozygous insulin receptor mutant mice for longevity phenotypes. Under 80% oxygen, mutant female mice survived 33.3% longer than wild-type female mice, whereas mutant male mice survived 18.2% longer than wild-type male mice. These results suggested that mutant mice acquired more resistance to oxidative stress, but the benefit of the longevity mutation was more pronounced in females than males. Manganese superoxide dismutase activity in mutant mice was significantly up-regulated, suggesting that the suppressed insulin signaling leads to an enhanced antioxidant defense. To analyze the molecular basis of the gender difference, we administered estrogen to mutant mice. It was found that the survival of mice under 80% oxygen was extended when they were administered estradiol. In contrast, mutant and wild-type female mice showed shortened survivals when their ovaries were removed. The influence of estrogen is remarkable in mutant mice compared with wild-type mice, suggesting that estrogen modulates insulin signaling in mutant mice. Furthermore, we showed additional extension of survival under oxidative conditions when their diet was restricted. Collectively, we show that three distinct signals; insulin, estrogen, and dietary signals work in independent and cooperative ways to enhance the resistance to oxidative stress in mice.

Recent experimental evidence suggests that oxidative stress is a principle cause of aging (1). Biochemical data further support the hypothesis that the oxidative damage accumulated in macromolecules such as DNAs, lipids, and proteins leads to the physiological decline in aging tissues. In a genetic analysis of invertebrate models, longevity mutants have been identified that show extension of lifespan associated with an enhanced resistance to oxidative stress (2). In *Caenorhabditis elegans*, a mutation of the *daf-2* gene that encodes an insulin/insulin-like growth factor type 1 (IGF-1)[1] receptor significantly enhanced resistance to oxidative stress and extended lifespan (3). These phenotypes are regulated by the insulin/IGF-1 signaling pathway from DAF-2 to DAF-16, a homologue of the hepatocyte nuclear factor-3/forkhead transcription factor (4, 5). Furthermore, expression of *sod3* encoding manganese superoxide dismutase (MnSOD) is up-regulated in *daf-2* mutants (5). In insulin-like signaling mutants of flies, it is suggested that the increased expression of SOD genes confers resistance to oxidative stress and the extension of lifespan (6). Thus, the regulation of SOD levels is critical for the determination of lifespan, which is modified by the insulin/IGF-1 signaling pathway. This signaling pathway has evidently been conserved from *C. elegans* to *Drosophila* (5, 6).

Holzenberger *et al.* (7) reported that a heterozygous deficiency for the IGF-1 receptor in mice enhances resistance to oxidative stress and extends lifespan. Because in IGF-1 receptor deficient mice heterozygous females exhibited a greater increase in lifespan than males, the beneficial effect of reduced IGF-1 signaling is also modulated by gender difference. However, it is unclear whether insulin signaling controls tolerance to oxidative stress and the extension of lifespan in mammals or is modulated by gender difference. In humans, the life expectancy of women is generally longer than that of men. For example, in Japan, with the highest life expectancy in the world, life expectancy was 78.36 years for men and 85.33 years for women in 2003. However, in laboratory animal models, the relationship of gender to longevity is variable, with lifespan being dependent on other factors like breeding and diet (8). Borras *et al.* (9) paid attention to the gender difference in rats, reporting that the expression and enzyme activity levels of MnSOD as well as glutathione peroxidase are higher in females than males. Ho *et al.* (10) reported that human MnSOD transgenic mice showed a significant increase in survival when exposed to 90% oxygen. Furthermore, in pulmonary epithelial cells of mice the overexpression of human MnSOD confers protection

* This work was supported by grants for Comprehensive Research on Aging and Health from the Ministry of Health, Labor, and Welfare. The costs of publication of this article were defrayed in part by the payment of page charges. This article must therefore be hereby marked "*advertisement*" in accordance with 18 U.S.C. Section 1734 solely to indicate this fact.

‖ Present address: Dept. of Developmental Genetics, Riken Research Center for Allergy and Immunology, Kanagawa, 230–0045, Japan.

** To whom correspondence should be addressed: Dept. of Molecular Gerontology, Tokyo Metropolitan Institute of Gerontology, 35-2 Sakaecho, Itabashi-ku, Tokyo 173-0015, Japan. Tel.: 81-3-3964-3241; Fax: 81-3-3579-4776; E-mail: sirasawa@tmig.or.jp.

[1] The abbreviations used are: IGF-1, insulin-like growth factor type 1; AL, *ad libitum*; Cu/ZnSOD, copper/zinc superoxide dismutase; MnSOD, manganese superoxide dismutase; DR, dietary restriction; E2, 17β-estradiol; IR, insulin receptor; OVX, ovariectomy; ROS, reactive oxygen species; wt, wild type; kb, kilobase; RT, reverse transcription.

against exposure to hyperoxygen (11). The regulation of antioxidant enzymes including MnSOD plays an important role in the determination of lifespan, suggesting that the gender difference in antioxidant enzymes explains the difference in life expectancy between females and males.

In the present study we generated a homologous murine model similar to the *daf-2* mutant ($Ir^{P1195L/wt}$) mouse in order to investigate the biological significance of longevity mutations found in the *daf-2* gene of *C. elegans*. We demonstrated that the mutant mice acquired an enhanced resistance to oxidative stress. Furthermore, we also revealed that the influence of gender difference and dietary restriction (DR) on the acquired resistance involved defective insulin signaling.

EXPERIMENTAL PROCEDURES

Generation of Insulin Receptor (IR) Mutant Mice—The 129 mouse genomic library in λFIXII (Stratagene, La Jolla, CA) was screened with rat IR cDNA containing exon 19–21 as a probe. Three overlapping clones covered exon 15–22 of the mouse IR gene. The 1.1-kb fragment containing exon 20 of the gene was PCR-amplified with two SpeI-anchored primers (5′-GGA CTA GTA GCA TTG AGA ACT GGA-3′ and 5′-GGA CTA GTA CCT GAG TTC AAT GCC A-3′). The SpeI-restricted fragment carrying exon 20 was mutagenized with a 19-bp mutagenic oligonucleotide (5′-GGA TGT CAC TCG AGT CCC T-3′) using the pALTER system (Promega, Madison, WI). The introduced mutation, P1195L, was confirmed present by sequencing. The 2.6-kb short 3′ homologous fragment was amplified with a XhoI-anchored primer (5′-CCG CTC GAG ATA GAG ACT ATT GTA CG-3′) and an ApaI/NotI-anchored primer (5′-ATG GGC CCG CGG CCG CTG TGA ACA TAC CTC TG-3′). XhoI/ApaI-restricted short 3′ homologous fragments were inserted into a XhoI/ApaI-restricted pBluescript II SK (pBSII SK, Stratagene) vector. The 1.3-kb MC1neo cassette flanked by the *lox*p sequence was PCR-amplified from a pMC1neo-lox vector (12) with a SalI-anchored primer (5′-CGC GTC GAC ATA ACT TCG TAT AAT G-3′) and a SalI/EcoRI-anchored primer (5′-CGC GTC GAC GAA TTC ATC GAT ACC GGC GAC ATA-3′). The SalI-restricted MC1neo-*lox*p cassette was inserted into a XhoI-restricted pBSII SK vector containing the short 3′ homologous fragment. The SmaI/SalI-restricted fragment including a mutagenized exon 20 was inserted into a SmaI/SalI-restricted pBSII SK vector containing a short 3′ homologous fragment and a MC1neo-*lox*p cassette. The 7.3-kb-long 5′ homologous fragment was PCR-amplified with a NotI-anchored primer (5′-ATT TGC GGC CGC TGG CTA ACA ACT GAC TC-3′) and an SmaI-anchored primer (5′-TCC CCC GGG TTT CTT GAG ACG AGC-3′). The NotI/SmaI-restricted long 5′ homologous fragment was inserted into a NotI/SmaI-restricted pMC1DT-A (Oriental Yeast, Tokyo, Japan). The resulting construct encompassing the fragment carrying a modified exon 20, the MC1neo-*lox*p cassette, and the short 3′ homologous fragment was restricted with NotI, blunted, and inserted into SmaI-restricted pMC1DT-A containing the long 5′ homologous fragment. The vector was then linearized with NotI and used for the electroporation of embryonic stem cells. Genomic DNAs from 240 G418-resistant embryonic stem clones were screened for homologous recombination by Southern blotting. One embryonic stem clone with the expected homologous recombination was used for generating chimeric mice by the aggregation method as described (13). The chimeric mice were cross-bred with C57BL/6CrSlc (Nihon SLC), and the germline transmission was confirmed by PCR amplification with the primers 5′-GCA TGT ATG TGG ACA CT-3′ and 5′-GTG GAG GTC ATG GTT GAG CA-3′ in agouti offspring. To analyze the sequence of the mutated allele in IR mutant mice, we prepared IR transcripts containing exons 19–21 from livers of homozygous embryos by reverse transcription (RT)-PCR using as primers 5′-GCG AAT TCA ATA ACC CAG GCC GCC CT-3′ and 5′-AGT CTC TCT GGA CAG TTA TCA-3′, as described below. We confirmed the presence of the introduced mutation, P1195L, and the absence of additional mutations in exon 20 of the transcripts by sequencing. To delete the neomycin resistance gene from the germline, we cross-bred heterozygous mice with CAG-Cre mice (kindly provided by Dr. Miyazaki, Osaka University) (14).

Animals were housed in specific pathogen-free facilities on a 12-h light/dark cycle (0800 on, 2000 off) and were fed a standard rodent chow (mouse diet CRF-1, Oriental Yeast, Tokyo) and water *ad libitum* (AL). All protocols for animal use and experiments were reviewed and approved by the Animal Care Committee of the Tokyo Metropolitan Institute of Gerontology.

Southern Blotting and PCR Analysis—For the knock-in allele, genomic DNA was digested with EcoRV, subjected to electrophoresis on a 0.7% agarose gel, and then transferred to a Hybond-N^+ nylon membrane (Amersham Biosciences). Probes were labeled with [α-^{32}P]dCTP (6000 Ci/mmol, Amersham Biosciences) using the Megaprime DNA labeling system (Amersham Biosciences). Membranes were hybridized with a HincII/HincII fragment as a 3′ probe, and the fragment was visualized using a Bioimage analyzer BAS-1000 (Fuji Film, Tokyo, Japan). To differentiate wild-type and mutated alleles, we amplified the genomic fragment harboring exons 20 and 21 by PCR with a sense primer (P1, 5′-GGA ATG ACA AGG GAC ATC TA-3′) and antisense primer (P2, 5′-CAC CTG TTC ATT AGA CAG GCC-3′). PCR products were then digested with EcoRI to separate wild-type and mutated alleles.

Tyrosine Kinase Assay of IR—Livers from day1 neonates were solubilized in 1% Triton X-100, 50 mM HEPES (pH 7.6), 150 mM NaCl, 10 μg/ml leupeptin, 10 μg/ml pepstatin, and 1 mM phenylmethylsulfonyl fluoride. The insoluble material was separated by ultracentrifugation at 100,000 × *g* for 1 h at 4 °C. The supernatant was applied to a wheat germ lectin-agarose column pre-equilibrated with buffer A containing 0.1% Triton X-100, 50 mM HEPES (pH 7.6), 150 mM NaCl, and protease inhibitors. The column was extensively washed using buffer A, and the bound glycoproteins, such as IR, were eluted in buffer A containing 0.3 M *N*-acetylglucosamine. Aliquots of eluate were incubated in the absence or presence of 0.1 nM insulin (Eli Lilly) for 1 h at room temperature. Thereafter, phosphorylation was initiated by the addition of 0.1 mCi of [γ-^{32}P]ATP in the presence of 0.1 nM ATP. After 20 min at room temperature, the reaction was stopped by the addition of stopping solution containing 0.1 M NaF, 4 mM $NaVO_3$, 1 mM EDTA, and 1 mM sodium pyrophosphate. Samples were immunoprecipitated with anti-IR antibody (kindly provided by Dr. Ebina, Tokushima University) (15) and protein A-Sepharose CL-4B (Amersham Biosciences). Labeled phosphoproteins were separated on sodium dodecyl sulfate, 10% polyacrylamide gels and detected by autoradiography.

Measurement of Protein Kinase B Phosphorylation—Mice were injected intravenously with 0.75 units kg^{-1} insulin or equal volume of vehicle. All tissues were collected in liquid nitrogen 5 min after the injection. Frozen tissues were homogenized with 6 (for muscle) or 10 (for liver and kidney) times the volume of the tissue in homogenization buffer (1% Triton X, 50 mM HEPES, pH 7.4, 100 mM sodium pyrophosphate, 100 mM NaF, 10 mM EDTA, 10 mM $NaVO_3$, and 2 mM phenylmethylsulfonyl fluoride). Phosphorylation at Ser-473 of protein kinase B in tissue extracts was analyzed with anti-phosphoprotein kinase B Ser-473 and anti-protein kinase B antibodies (Cell Signaling) as described (16).

Oxidative Stress—Twenty (4-month-old) mice were continuously exposed to 80% oxygen for 14 days in a chamber (50 × 30 × 30 cm). The concentration of fractional inspired O_2 in the chamber was monitored with an oxygen analyzer (G-101-Y, Iijima Products, Gamagouri, Japan) and maintained with a constant flow of 80% oxygen gas (3 liters/min). Exposure was continuous for the time indicated except for a few minutes when the chamber was opened for housekeeping purposes weekly. The mice were fed food and water *ad libitum* and kept on a 12-h dark-light cycle at 25 °C. We checked the survival of mice every 12 h. As chemical oxidative stress, the mice (4-month-old) were intraperitoneally injected with paraquat (Sigma) prepared in phosphate-buffered saline at a dose of 70 mg/kg of body weight. We checked the survival of mice every 2 h until 120 h after the injection.

Analytical Procedures—Blood glucose levels were determined in fed mice (3, 6, and 12 months old) using an automatic monitor, Gluco-card (Hoechst Marion Roussel). Serum insulin levels were measured in 16-week-old mice. Serum obtained from fed mice was analyzed for insulin using a mouse insulin enzyme-linked immunosorbent assay kit (Shibayagi, Japan). In glucose tolerance tests fasting (4-month-old) mice were injected intraperitoneally with 2 g/kg body weight of 20% D-glucose. Blood glucose values were determined in whole blood obtained from the tail at 0, 15, 30, 60, and 120 min after the glucose injection. In insulin tolerance tests, 4-month-old mice were injected intraperitoneally with 1 units/kg of body weight of insulin. Blood glucose values were measured at 0, 15, 30, and 60 min after the injection.

SOD Activity Assay—Livers were homogenized in phosphate-buffered saline, pH 7.4, containing 2 mM EDTA, 2 mM EGTA, 2 mM phenylmethylsulfonyl fluoride, and 4 μg/ml leupeptin, then sonicated 10 times using the handy sonicator. The lysates were spun at 15,000 × *g* for 30 min to remove cell debris. SOD activity was measured by a competitive assay as described previously (17). The amount of protein that inhibits the tetrazolium dye WST-1 (Dojindo, Kumamoto, Japan) reduction to 50% of maximum is defined as 1 unit of SOD activity. Enzymatic activity was expressed in units per mg of protein. To measure MnSOD activity, KCN was added to tissue lysates at a final concentration of 1 mM to inhibit the cupper/zinc (Cu/Zn) SOD activity.

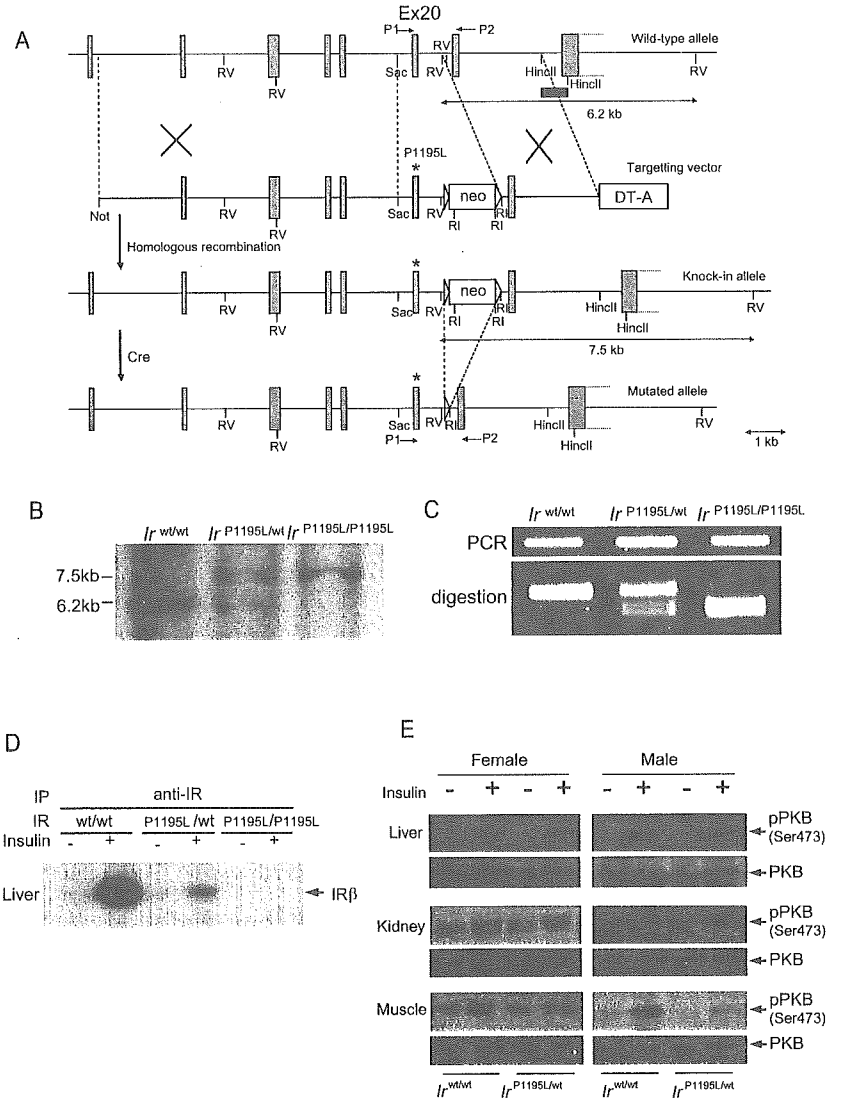

FIG. 1. **Generation of IR mutant mice.** *A*, strategy used to knock-in the IR mutation (P1195L) in the murine IR gene locus. Diagrams of the murine IR genome locus, targeting vector, knock-in allele, and mutated allele are presented. The *open boxes* indicate the neomycin resistance cassette (*neo*) and DT-A gene. Exons are indicated as *solid boxes*. *Open triangles* represent *lox*p sequences. After the cross-breeding with Cre-expressing transgenic mice, the neo cassette was popped out from the genome (mutated allele). The probe for Southern blotting is shown as a *black box*. The *arrows* indicate primers P1 and P2 for PCR. *RI*, EcoRI; *RV*, EcoRV. *B*, Southern blot analysis of EcoRV-digested liver DNAs in embryos. The knock-in allele yielded a 7.5-kbp EcoRV fragment, whereas the wild-type allele yielded a 6.2-kbp EcoRV fragment. *C*, PCR-based genotyping of $Ir^{wt/wt}$, $Ir^{P1195L/wt}$, and $Ir^{P1195L/P1195L}$ embryos. Products amplified with primers P1 and P2 were digested by EcoRI to identify wild-type and mutated alleles. *D*, insulin-induced IR phosphorylation in liver of IR mutant mice. *E*, insulin-induced protein kinase B (*PKB*) phosphorylation in liver, kidney, and muscle of IR mutant mice.

Reverse Transcription (RT)-PCR—Tissues were homogenized in Trizol reagent (Invitrogen). Total RNA was extracted according to the manufacturer's instructions. cDNA was synthesized by reverse transcriptase from 1 μg of total RNA using a RNA PCR kit (Takara Bio Inc., Japan). Mouse MnSOD, Cu/ZnSOD, and glyceraldehyde-3-phosphate dehydrogenase cDNAs were amplified using specific oligonucleotide primers (MnSOD, 5′-GAC CTG CCT TAC GAC TAT GG-3′ and 5′-GAC CTT GCT CCT TAT TGA AGC-3′; Cu/ZnSOD, 5′-ATG AAA GCG GTG TGC GTG CTG-3′ and 5′-AAT CAC TCC ACA GGC CAA GCG-3′; glyceraldehyde-3-phosphate dehydrogenase, 5′-TCG GTG TGA ACG GAT TTG GC-3′ and 5′-ATT TCT CGT GGT TCA CAC CC-3′). PCR products were electrophoresed and visualized using ethidium bromide.

Ovariectomy (OVX) and Estradiol (E2) Administration—At 12 weeks of age, female mice were ovariectomized or sham-operated via a midline incision under anesthesia with pentobarbital (40 mg/kg, intraperitoneal injection). After 4 weeks, treated mice were exposed to 80% oxygen or SOD activity, and gene expression levels were analyzed. Male (12-week-old) mice and OVX female (16-week-old) mice were administered a weekly subcutaneous injection of 17β-estradiol (20 mg/kg per week; Sigma) in corn oil (Ajinomoto, Japan). After 4 weeks of treatment, the male and female mice were exposed to 80% oxygen. E2-treated male mice were analyzed for SOD activity and gene expression.

DR—At 16 weeks of age we measured food intake per day in male and female mice and randomly assigned the mice to two groups, AL and DR. Four mice were housed in every cage (20 × 10 × 20 cm). The mice in the AL group were fed freely, whereas those in the DR group were fed a restricted diet on Monday, Wednesday, and Friday. First, DR mice were fed a 10%-restricted diet for a week, and then the restricted diet was gradually reduced by 65% for 3 weeks. Finally, DR consisted of 65% of food intake in AL mice. We adjusted the amount of restricted diet by measuring food intake in AL mice every 10 weeks. We housed DR mice until the age of 60 weeks.

RESULTS

The Generation of Modified IR Mutant Mice—To elucidate the biological significance of the longevity mutation found in the *daf*-2 mutant of *C. elegans*, we generated a homologous murine model by replacing Pro-1195 of IR with Leu by targeted knock-in of the genomic IR gene in mice. As shown in Fig. 1*A*, we first isolated an ES cell carrying a mutation homologous to *daf-2* (*e1391*) (3), *i.e.* Leu-1195 in exon 20 of the IR genomic gene by homologous recombination with the target vector. Germline transmission was confirmed in the F1 offspring of the chimeric and C57BLACK/6 mice by Southern blotting. As shown in Fig. 1*B*, the blot showed that the 3′ probe detected a 6.2-kb polymorphic EcoRV allele in wild-type ($Ir^{wt/wt}$) as well as heterozygous ($Ir^{P1195L/wt}$) mice, whereas the probe detected a 7.5-kb mutant EcoRV allele in heterozygous and homozygous ($Ir^{P1195L/P1195L}$) mice. To delete the neomycin resistance gene from the germline, we cross-bred $Ir^{P1195L/wt}$ mice with CAG-Cre mice (14). We successfully deleted the neomycin resistance gene from the germline by cross-breeding CAG-Cre mice as schematized in the *bottom* of Fig. 1*A*. To detect the wild-type and mutant alleles, we amplified the genomic fragment harboring exon 20 and 21 by PCR with a sense primer (P1) and an antisense primer (P2). The PCR products were then differentiated based on the EcoRI site that is specifically introduced with

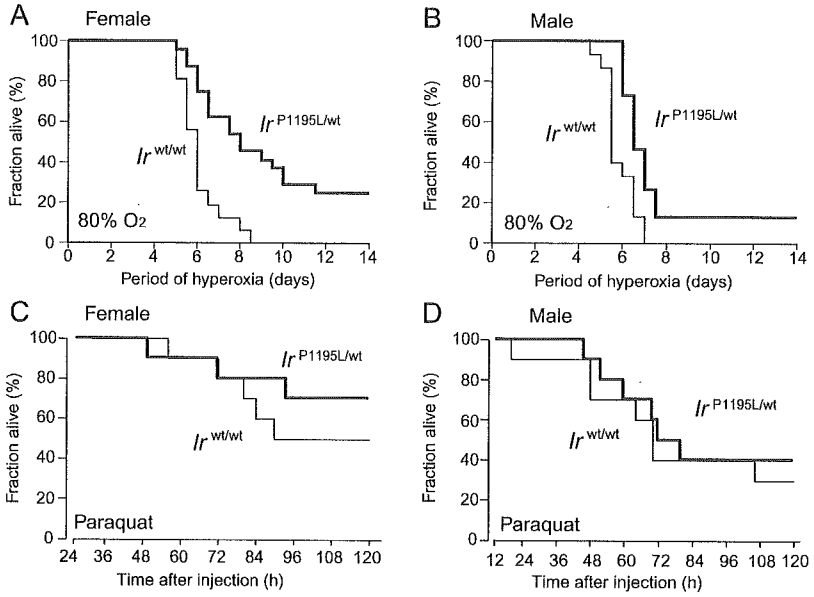

FIG. 2. **IR mutant mice at 4 months of age show resistance to oxidative stress.** *A* and *B*, oxidative stress was induced by exposure to 80% oxygen. Kaplan-Meier analysis showed a significant increase in survival of $Ir^{P1195L/wt}$ compared with $Ir^{wt/wt}$ mice. Female mutants exhibited increased stress resistance ($p < 0.005$, g-Wilcoxon test, at least 16 mice per genotype), whereas male mutants showed a significant increase ($p < 0.05$, g-Wilcoxon test, at least 15 mice per genotype). *C* and *D*, paraquat was injected. $Ir^{P1195L/wt}$ female mice survived longer than wild-type mice beyond 72 h. IR mutant male mice also survived longer than wild-type mice (not significant, g-Wilcoxon test, $n = 10$ in each group).

the knock-in allele (Fig. 1*C*). A genotypic analysis of the offspring showed that the frequency of wild-type, heterozygous and homozygous mice was 31:61:0 at the 4-week-old stage. Further observation, however, showed that some mice were identified as homozygous at 1 day old, which apparently showed that the growth retardation was complicated by the diabetic ketoacidosis.[2] The result suggested that the homozygous mice failed to thrive due to diabetic ketoacidosis in the neonatal stage, which is consistent with the phenotypes previously reported in IR-deficient mice (18, 19).

To investigate the autophosphorylation activity of IR in IR mutant mice, insulin was added to extracts from the neonatal liver of the mice. As shown in Fig. 1*D*, we did not detect any insulin-induced autophosphorylation activity in the $Ir^{P1195L/P1195L}$ mouse. On the other hand, the $Ir^{P1195L/wt}$ mouse did show the insulin-induced autophosphorylation although it was less than 20% that of the $Ir^{wt/wt}$ mouse. Furthermore, to investigate whether the downstream activity of IR is suppressed by the mutation of the IR gene, we monitored protein kinase B phosphorylation, a more distal event in IR signaling (Fig. 1*E*). As with IR autophosphorylation in $Ir^{P1195L/wt}$ mice, insulin-induced protein kinase B phosphorylation was suppressed in liver, kidney, and muscle of $Ir^{P1195L/wt}$ mice compared with $Ir^{wt/wt}$ mice (Fig. 1*E*). These results indicated that the tyrosine kinase activity of IR from heterozygous ($Ir^{P1195L/wt}$) mice was severely suppressed in a dominant negative manner, suggesting that IR mutant mice provide an excellent model for the analysis of longevity phenotypes induced by suppressed insulin signaling compared with heterozygous IR-deficient mice with a haploinsufficiency of insulin signal.

IR Mutant Mice Showed Enhanced Resistance to Oxidative Stress—To investigate whether IR mutant mice acquired enhanced resistance to oxidative stress, the mice at 4 months of age were exposed to 80% oxygen in a chamber. We then compared the survival of IR mutant mice to that of wild-type mice (Fig. 2). IR mutant females survived 33.3% longer than female wild-type mice, *i.e.* IR mutant mice had a 50% survival rate at 8 days compared with 6 days for wild-type mice (Fig. 2*A*). On the other hand IR male mutant mice survived 18.2% longer than wild-type male mice, *i.e.* IR mutant mice had a 50% survival rate at 6.5 days compared with 5.5 days for wild-type mice (Fig. 2*B*). These results suggested that IR mutant mice are more resistant to oxidative stress, but the benefit of the mutation was more pronounced in female than male mice.

Next, we intraperitoneally injected paraquat, a chemical oxidant, into female and male mice to evaluate the defense system of the mutant mice against chemically induced oxidative stress. As shown in Fig. 2*C*, both IR mutant and wild-type female mice began to die ~48 h after the administration of paraquat. IR mutant female mice, however, survived significantly longer than wild-type mice in stages beyond 72 h. IR mutant male mice also survived longer than wild-type mice, but the beneficial effects in male mutant mice were less pronounced in comparison to those in female mutant mice (Fig. 2*D*). These results suggested that IR mutant mice of both genders survived longer than wild-type mice in oxidative conditions. It is also of note that there is a gender difference in the resistance to oxidative stress in IR mutant mice. This data suggested that the insulin signaling may be modulated by sex hormones (*i.e.* either by the beneficial effects of estrogen or by the deleterious effects of testosterone).

MnSOD Plays a Role in the Acquisition of Resistance to Oxidative Stress—Because MnSOD and Cu/ZnSOD play an important role in the intracellular defense against reactive oxygen species (ROS), we measured SOD activities in the liver of IR mutant mice. As shown in Fig. 3*A*, the MnSOD activity of IR mutant female mice was significantly up-regulated by 39.9% compared with that of wild-type female mice (484.9 ± 96.1 units/mg of protein for IR mutant mice *versus* 346.5 ± 51.7 units/mg of protein for wild-type mice, $p < 0.05$). As for male mutant mice, MnSOD activity was up-regulated by 22.9% in comparison with that of wild-type male mice, but the up-regulation was less significant than that found in wild-type female mice (Fig. 3*B*). In contrast, we did not detect any pronounced difference in Cu/ZnSOD activity between IR mutant and wild-type mice of either sex (Fig. 3, *C* and *D*). To analyze the molecular basis for the up-regulation of MnSOD, mRNAs for MnSOD and Cu/ZnSOD were analyzed by RT-PCR (Fig. 3*E*). We found that the transcription of MnSOD was up-regulated in liver, brain, kidney, and heart of both female and male mutant mice, whereas that of the Cu/ZnSOD and glyceraldehyde-3-phosphate dehydrogenase genes was not up-regulated in mutant or wild-type mice (Fig. 3*E*). Furthermore, to investigate the contribution of other antioxidant enzymes to resistance to oxidative stress, we measured activities of glutathione peroxi-

[2] T. Baba, T. Shimizu, Y. Suzuki, H. Koseki, and T. Shirasawa, manuscript in preparation.

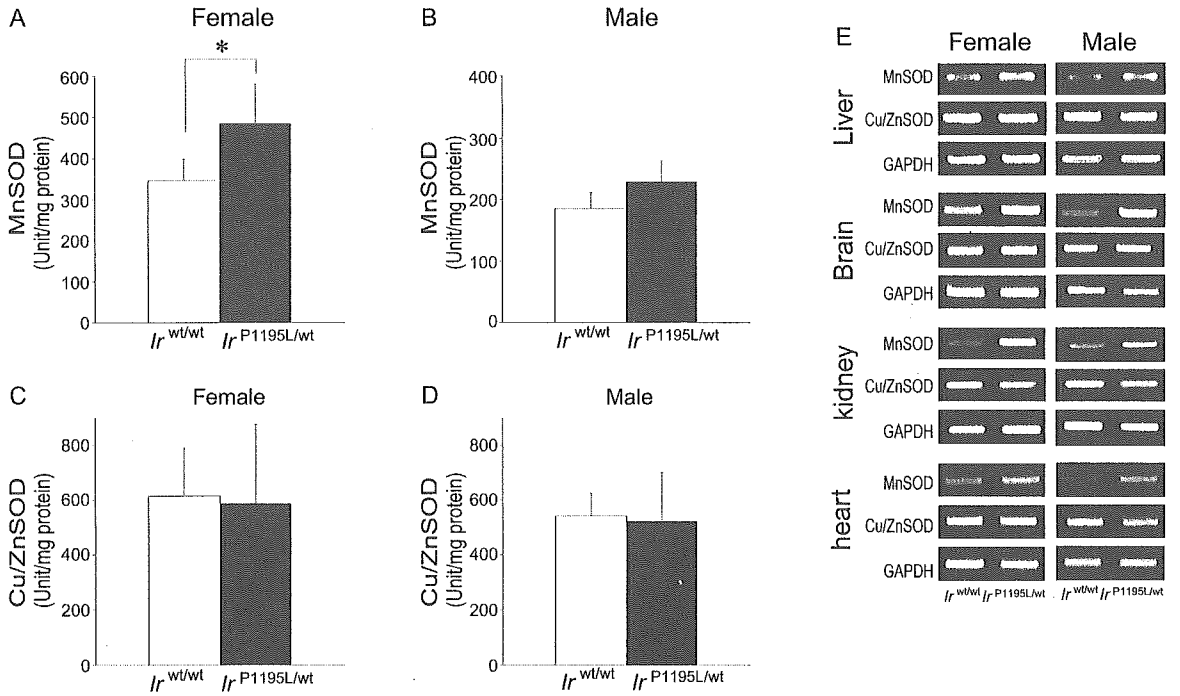

FIG. 3. **The expression and activities of antioxidant enzymes.** *A*, MnSOD activity was significantly stronger in $Ir^{P1195L/wt}$ female mice than $Ir^{wt/wt}$ female mice. *B*, $Ir^{P1195L/wt}$ male mice showed higher levels of MnSOD activity than $Ir^{wt/wt}$ male mice but not significantly so. *C* and *D*, Cu/ZnSOD activity was not up-regulated in mutant mice. *E*, RT-PCR analysis. Expression of the MnSOD gene was stronger in liver, brain, kidney, and heart of $Ir^{P1195L/wt}$ male and female mice than $Ir^{wt/wt}$ mice. Expression of the Cu/ZnSOD gene was not up-regulated in mutant mice. The glyceraldehyde-3-phosphate dehydrogenase (*GAPDH*) gene as an internal control is shown. Each *bar* represents the mean ± S.D. in each group from at least five mice per genotype. *, $p < 0.05$; $Ir^{P1195L/wt}$ mice *versus* $Ir^{wt/wt}$ mice.

dase and catalase. However, we did not detect any significant differences between IR mutant and wild-type mice (data not shown). These results suggested that the transcriptional up-regulation of MnSOD is specific to the enhanced antioxidant system in IR mutant mice. In *C. elegans* and *Drosophila melanogaster*, the up-regulated SODs are reported to degrade the oxygen radicals that cause oxidative stress in IR/ IGF-1 receptor mutants (5, 6, 20). Kops *et al.* (21) reported that MnSOD was up-regulated upon treatment with insulin in cultured 3T3-L6 cells. Here we demonstrated for the first time that the expression and the activity of MnSOD were up-regulated by the mutation introduced into the kinase domain of the IR gene in mice. Transgenic flies, which overexpressed Cu/ZnSOD in motor neurons, survived 40% longer than control fruit flies, whereas transgenic flies that overexpressed MnSOD in motor neurons survived 30% longer than control flies (22, 23). The up-regulation of MnSOD may confer an extension of lifespan in *Drosophila*. The regulation of MnSOD by insulin signaling was shown to be conserved between invertebrates and mammals, suggesting that the antioxidant system against ROS plays an important role in the determination of animal lifespan in both invertebrates and vertebrates.

Estrogen Signaling Enhances Tolerance to Oxidative Stress in IR Mutant Mice—The MnSOD activity of female mice was significantly up-regulated in comparison with that of male mice (Fig. 3, *A* and *B*). Strehlow *et al.* (24) reported that the gene expression of MnSOD and extracellular SOD in ovariectomized mice was down-regulated to 40–60% that of the control level and was recovered through estrogen replacement therapy (24). To investigate whether estrogen signaling confers resistance to oxidative stress and up-regulates MnSOD expression in IR mutant mice, we performed OVXs on female mice. For male mice, on the other hand, we administered E2 for 4 weeks.

First, we investigated the oxidative tolerance under hyperoxic conditions and the activity of MnSOD in the liver of OVX mice. As shown in Fig. 4, *A* and *B*, we compared the survival rate of OVX mice with that of non-OVX mice in both the IR mutant mice and wild-type strains. OVX mutant mice died significantly earlier than non-OVX mutant mice, *i.e.* OVX mutant mice had a 50% survival rate at 6.5 days compared with 12 days for non-OVX mutant mice (Fig. 4*A*). OVX wild-type mice died earlier than non-OVX wild-type mice, *i.e.* OVX wild-type mice had a 50% survival rate at 5.5 days compared with 7 days for non-OVX wild-type mice (Fig. 4*B*). The shortening of the survival rate was more pronounced in IR mutant mice than the wild-type mice, when both were ovariectomized. To clarify the molecular mechanisms of shortened survival in OVX mice, we investigated the gene expression and enzyme activity of MnSOD in the liver of mutant mice. As shown in Fig. 5*A*, the MnSOD activity of IR mutant mice was significantly down-regulated upon OVX (484.9 ± 96.1 units/mg of protein for mutant mice *versus* 387.3 ± 88.9 units/mg of protein for OVX mutant mice, $p < 0.05$). The down-regulation of MnSOD activity was less pronounced in wild-type OVX mice. In contrast, we did not detect any difference in Cu/ZnSOD activity upon OVX (Fig. 5*C*). The transcription of MnSOD was significantly down-regulated in OVX mice (Fig. 5*E*).

Second, to investigate the influence of exogenous estrogen on male mice, we administered E2. After exposure to 80% oxygen, we compared the survival of males treated with E2 to that of untreated make of both IR mutant mice and wild-type mice. Interestingly, mutant males administered E2 survived significantly longer than untreated mutant mice (Fig. 4*E*). The extension of survival was more pronounced in IR mutant mice than wild-type mice, when both were administered estrogen (Fig. 4, *E* and *F*). As shown in Fig. 5*B*, MnSOD activity was up-regulated by 20.6% in IR mutant mice treated with E2. The MnSOD activity of wild-type male mice was also up-regulated by 15.3% upon administration of E2. In contrast, we found no up-regulation of Cu/ZnSOD activity with E2 administration. (Fig. 5*D*). The transcription of MnSOD was significantly up-regulated in male mice administered E2 (Fig. 5*F*).

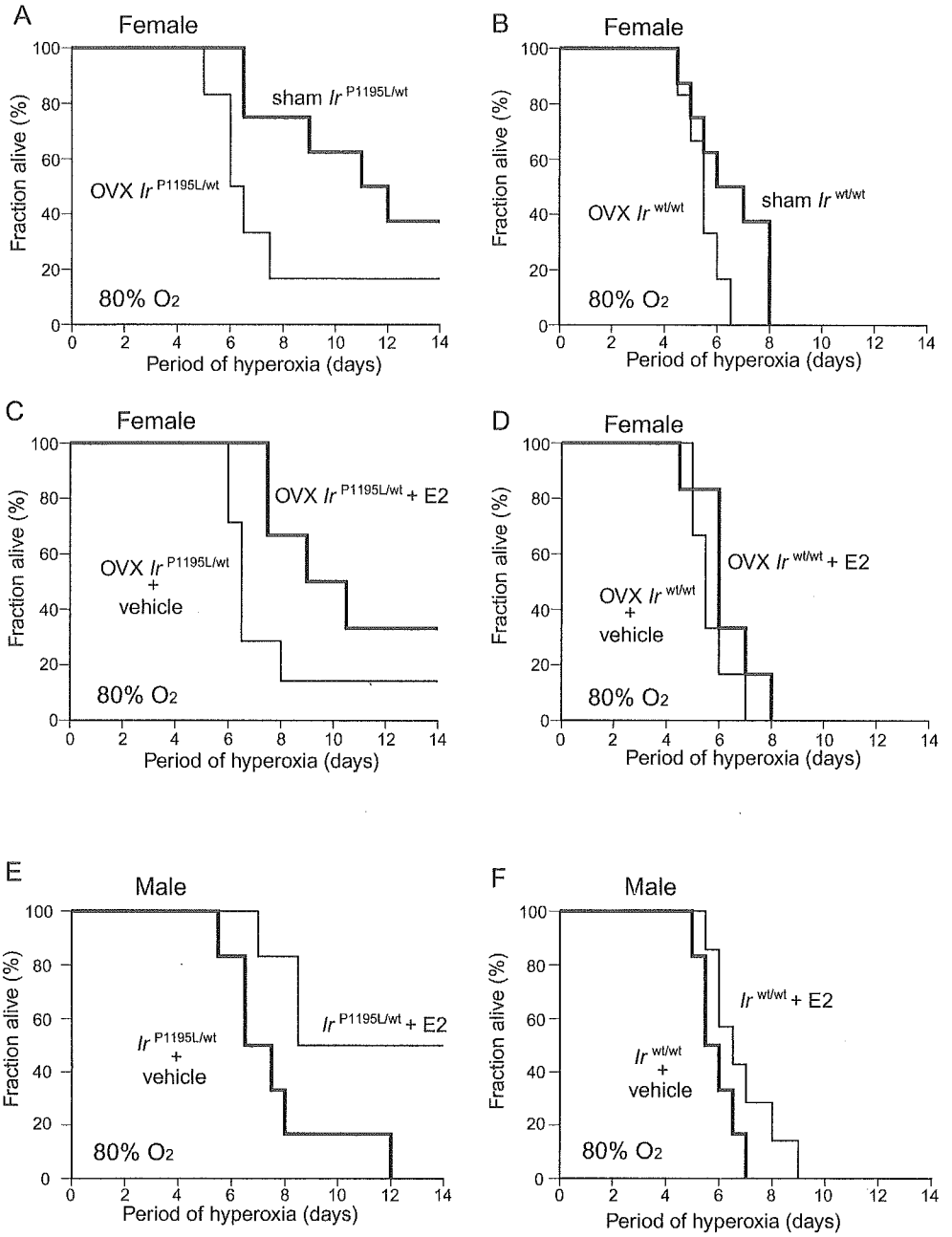

FIG. 4. **Estrogen signaling enhances resistance to oxidative stress in $Ir^{P1195L/wt}$ mice.** *A* and *B*, OVX mice died earlier than non-OVX mice. The shortening of the survival period was greater in $Ir^{P1195L/wt}$ mice ($p < 0.05$, g-Wilcoxon test) than $Ir^{wt/wt}$ mice (not significant, g-Wilcoxon test). *C* and *D*, estrogen replacement improved the resistance to oxidative stress in OVX mice. The influence of E2 was remarkable in $Ir^{P1195L/wt}$ female mice ($p < 0.05$, g-Wilcoxon test) compared with $Ir^{wt/wt}$ mice (not significant, g-Wilcoxon test) upon OVX. *E* and *F*, male mice treated with E2 survived longer than untreated mice. The influence of E2 was remarkable in $Ir^{P1195L/wt}$ male mice ($p < 0.05$, g-Wilcoxon test) compared with $Ir^{wt/wt}$ mice (not significant, g-Wilcoxon test).

Finally, to exclude the possibility that the deficiency of testosterone caused by the feedback regulation of E2 administration is attributable to the phenotype of E2-treated males, we investigated the influence of exogenous estrogen on OVX mice. After 4 weeks of E2 administration, OVX mice were exposed to 80% oxygen. OVX mutant mice treated with E2 survived significantly longer than untreated mutant mice; the E2-treated group had 50% survival at 10.5 days compared with 6.5 days for the untreated group (Fig. 4*C*). OVX wild-type mice treated with E2 also survived longer than untreated wild-type male mice but not significantly so (Fig. 4*D*). We demonstrated here that mutant mice administered E2 survived longer with hyperoxygen as well as showed an up-regulation of MnSOD expression. Interestingly, the influence of estrogen was remarkable on IR mutant mice compared with wild-type mice.

The Gender Difference of Glucose Metabolism in IR Mutant Mice—To determine whether the suppression of IR signaling induces an impairment of glucose metabolism, levels of glucose (Fig. 6*A*) and insulin (Fig. 6*B*) were analyzed in blood samples. In a fed state, IR mutant mice had almost the same blood glucose concentrations as wild-type mice. However, about 6% of mutant male mice developed hyperglycemia (more than 200 mg/dl) (Fig. 6*A*). This rate was the same as in mice heterozygous for insulin receptor knock-out (25). In contrast, we did not detect any differences in urinary glucose between mutant and wild-type mice (data not shown). Serum insulin concentrations in the fed state were significantly increased in both female and male mutant mice compared with wild-type mice (Fig. 6*B*).

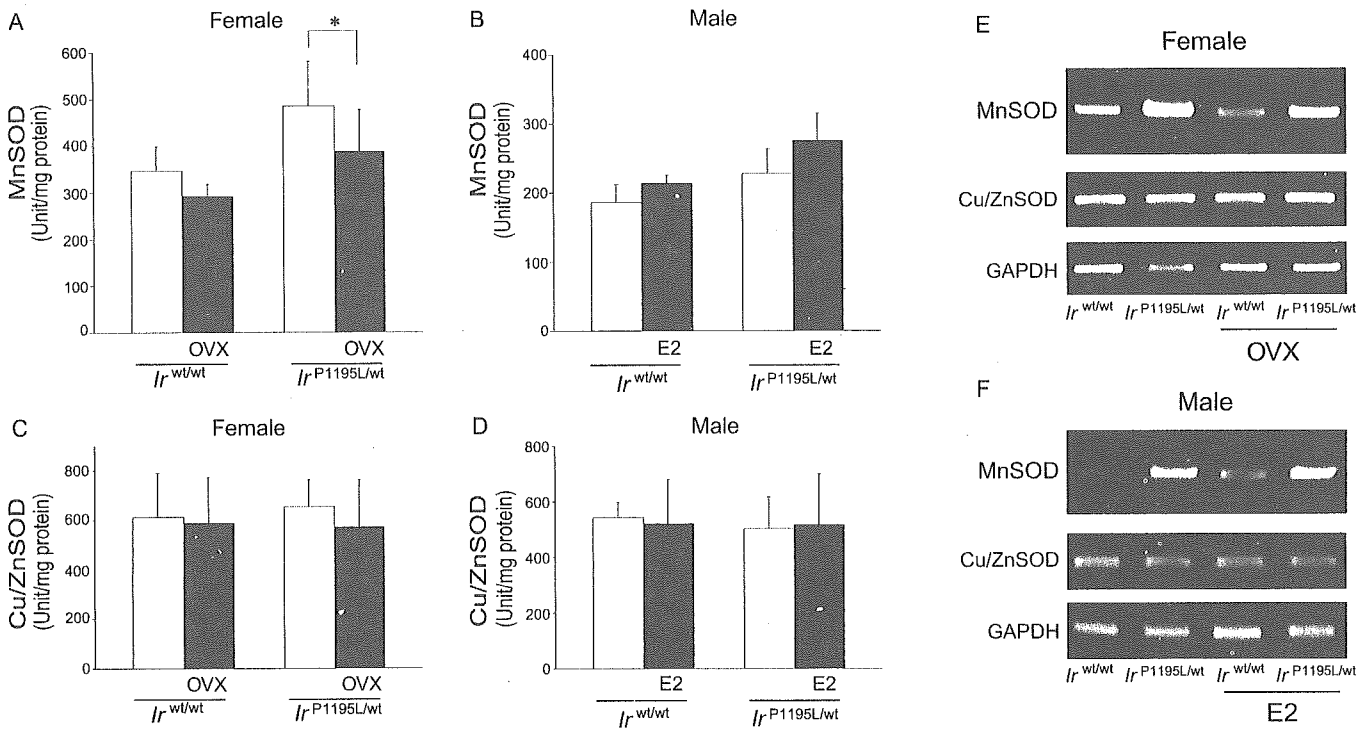

FIG. 5. **Activities and transcriptional expression of antioxidant enzymes.** *A*, MnSOD activity was down-regulated in OVX female mice. *B*, MnSOD activity was up-regulated in male mice when exogenous E2 was administered. *C* and *D*, Cu/ZnSOD activity was not up-regulated in OVX or E2-administered mutant mice. *E* and *F*, MnSOD transcription in the RT-PCR analysis was down-regulated upon OVX in female mice and up-regulated in male mice treated with E2. Each *bar* represents the mean ± S.D. in each group from at least five mice per genotype. *, $p < 0.05$; $Ir^{P1195L/wt}$ mice *versus* $Ir^{wt/wt}$ mice. *GAPDH*, glyceraldehyde-3-phosphate dehydrogenase.

Although we failed to detect any gender difference in insulin concentrations of wild-type mice, insulin concentrations were significantly increased in IR mutant males (6.40 ± 1.49 ng/ml) compared with IR mutant females (2.96 ± 1.63 ng/ml) (Fig. 6*B*).

To determine the physiological consequence of mutated IR, glucose and insulin tolerance tests were performed on 4-month-old mice. Both female and male IR mutant mice showed normal fasting blood glucose concentrations as compared with control mice (Fig. 6, *C* and *D*). However, IR mutant male mice showed a moderately impaired glucose tolerance as compared with control male mice (Fig. 6*D*), whereas IR mutant female mice showed normal glucose tolerance (Fig. 6*C*). In addition, IR mutant females were more sensitive to blood glucose-lowering effects than wild-type mice when insulin was administered (Fig. 6*E*). In contrast, IR mutant male mice showed resistance to blood glucose-lowering effects in the insulin tolerance test (Fig. 6*F*). Although IR signaling was suppressed in IR mutant mice, mutant females sustained insulin sensitivity with hyperinsulinemia. This gender difference suggested that sex hormones may modulate the insulin signaling in IR mutant mice.

Then, to investigate whether sex hormones influence glucose metabolism, glucose and insulin tolerance tests were performed on female OVX mice and male mice treated with E2. Upon OVX, the glucose tolerance of IR mutant mice showed no significant changes as compared with that of wild-type mice (Fig. 6*G*). However, OVX mutant mice showed impaired insulin sensitivity compared with non-OVX mutant mice (Fig. 6, *E* and *I*). Furthermore, E2 administration improved glucose intolerance and insulin resistance in IR mutant male mice (Fig. 6, *H* and *J* compared with *D* and *F*). In contrast, wild-type mice showed no significant changes upon the administration of E2.

As for the mechanism of action of estrogen, Pedersen *et al.* (26) reported that IR binding was increased in adipocytes from rodents treated with estrogen. In that case, IR binding seemed to be due to an increased number of IRs (26). Yu *et al.* (27) reported that an IR signaling pathway is involved in estrogen-mediated retinal neuroprotection. The influence of estrogen is remarkable on IR mutant mice when compared with wild-type mice, suggesting that estrogen partially enhances its effect through insulin signaling.

DR Additively Enhances the Resistance against Oxidative Stress in IR Mutant Mice—Dietary restrictions that facilitate a reduction in body weight, mainly fat mass, are known to prolong lifespan by enhancing resistance against oxidative stress in mammals (28–30). Bluher *et al.* reported that fat-specific insulin receptor knock-out mice showed reduced adiposity, suggesting that the reduction of fat mass may be beneficial for the extension of lifespan (31, 32). To clarify whether there is a reduction of adipose tissue induced by mutation in the IR gene, we observed whole body and organ weights of IR mutant mice. Both male and female IR mutant mice sustained a significant 10–15% reduction in body weight compared with wild-type mice (Fig. 6, *A* and *B*). The fat mass of IR female mutant mice decreased significantly by 41.3% when compared with wild-type mice (446.6 ± 36.1 *versus* 761.4 ± 183.0 mg, $p < 0.05$), whereas that of IR male mutant mice dropped significantly by 57.5% compared with wild-type mice (522.9 ± 54.7 *versus* 1230.0 ± 196.0 mg, $p < 0.01$). We found no difference in the weights of other organs between IR mutant and wild-type mice (Fig. 6, *A* and *B*). To exclude the possibility that IR mutant mice show reduced food intake, we measured the food intake of mice at age of 16 weeks. We did not detect any significance difference in food intake between wild-type and mutant mice (female; 3.37 ± 0.1 *versus* 3.45 ± 0.18 g/day, male; 3.54 ± 0.11 *versus* 3.57 ± 0.15 g/day). We demonstrated that IR mutant mice specifically exhibited a reduction in fat mass, suggesting that the phenotype of IR mutant mice is very similar to that of fat-specific insulin receptor knock-out mice (31, 32).

To elucidate the influence of DR in IR mutant mice, the diet was restricted to 65% that consumed by the mice fed *ad libi-*

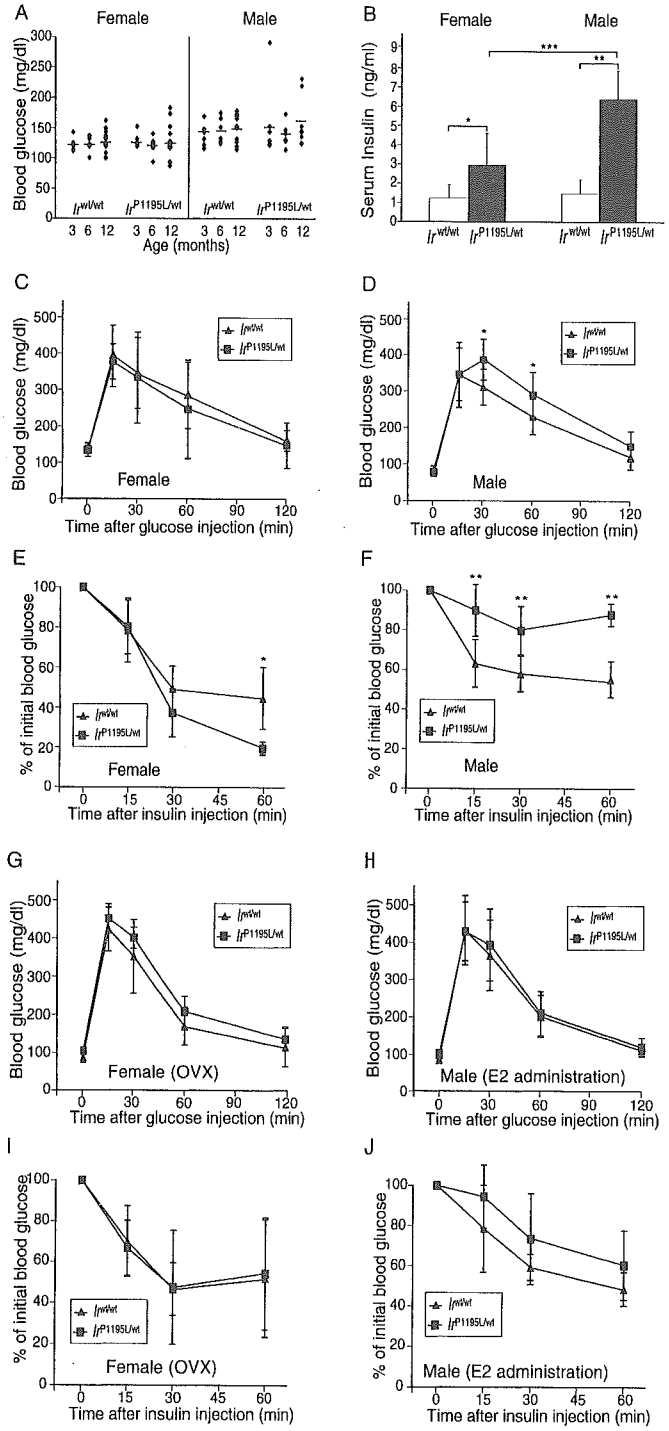

FIG. 6. **The gender difference of glucose metabolism in IR mutant mice.** *A*, most $Ir^{P1195L/wt}$ mice exhibited blood glucose concentrations within the range of $Ir^{wt/wt}$ mice. *B*, insulin concentrations were significantly increased in $Ir^{P1195L/wt}$ male mice as compared with $Ir^{P1195L/wt}$ female mice. *C* and *D*, glucose tolerance tests performed on 4-month-old $Ir^{P1195L/wt}$ mice. We did not detect any differences in glucose tolerance between $Ir^{P1195L/wt}$ and $Ir^{wt/wt}$ female mice (C). $Ir^{P1195L/wt}$ male mice showed moderately impaired glucose tolerance compared with $Ir^{wt/wt}$ male mice (*D*). *E* and *F*, insulin tolerance tests were performed on random-fed, 4-month-old $Ir^{P1195L/wt}$ mice. The testing demonstrated that $Ir^{P1195L/wt}$ female mice were more sensitive to insulin than $Ir^{wt/wt}$ female mice (*E*). $Ir^{P1195L/wt}$ male mice were resistant to insulin (*F*). Upon OVX, glucose tolerance of $Ir^{P1195L/wt}$ mice showed no significant change as compared with that of $Ir^{wt/wt}$ mice (*G*). OVX $Ir^{P1195L/wt}$ mice showed an impaired insulin sensitivity compared with non-OVX mice (*I*). E2 administration improved glucose intolerance and insulin resistance in $Ir^{P1195L/wt}$ male mice (*H* and *J*). Each *bar* represents the mean ± S.D. in each group from at least six mice per genotype. *, $p < 0.05$; **, $p < 0.01$; ***, $p < 0.005$; $Ir^{P1195L/wt}$ mice *versus* $Ir^{wt/wt}$ mice.

tum. As a result, IR mutant female mice with DR showed a 78.9% reduction of fat mass compared with AL wild-type mice, whereas the mutant males with DR showed an 88.4% reduction (Fig. 7, *A* and *B*). Although IR mutant and wild-type mice with DR also showed a reduction in the weights of other tissues, it was not as remarkable as that observed in fat mass. We demonstrated that genetic manipulation further enhances the reduction of fat mass induced by DR.

To clarify the influence of the reduction in fat tissue in IR mutant mice, we exposed IR mutant and wild-type mice to 80% oxygen. Interestingly, IR mutant mice showed a comparable survival rate to wild-type mice with DR (Fig. 7, *C* and *D*). The result suggested that genetic factors as well as DR independently play an important role, although we could not rule out cross talk between them. Surprisingly, IR mutant female and male mice both showed an extended lifespan upon DR (Fig. 7, *C* and *D*). Houthoofd *et al.* (33) reported that lifespan extension via DR is independent of the insulin/IGF-1 signaling pathway in *C. elegans*. Although the reduction of fat mass induced by DR is more pronounced in mutant males than females, IR mutant female mice survived longer than IR mutant male mice under oxidative conditions. These results indicated that IR mutant female mice showed beneficial effects of DR as well as endogenous estrogen for the resistance to oxidative stress.

DISCUSSION

MnSOD Is Up-regulated in Vivo in IR Mutant Mice—Daf-2 is one of the longevity mutants found in *C. elegans* (3). The causative mutation was found in the gene encoding the insulin-like receptor, suggesting that the *daf-2* mutant has a defective insulin-like signaling, which eventually triggers the dauer formation as well as the extension of lifespan in *C. elegans* (3, 4). The mutation of *daf-16*, a major suppressor mutant for *daf-2*, was found in the gene encoding the forkhead transcription factor (34, 35). Biochemical analyses revealed that DAF-16, or dFOXO of the fly ortholog, played a pivotal role as a transcription factor by regulating the longevity genes downstream of the insulin signaling pathway (34–36). The signaling pathway triggered by insulin or insulin-like ligands is well conserved among various animal species, including mammals and invertebrates such as *D. melanogaster*, in which mutants for the insulin receptor, *IR*, or *IRS-1*, *chico*, also exhibit the longevity phenotype (6, 20). One of the candidate longevity genes in the downstream of *daf-16* is the MnSOD gene (37), whose expression is specifically up-regulated in *daf-2* mutants (5). Because biochemical studies show that MnSOD catalyzes the superoxide endogenously generated in the mitochondrial matrix, the balance between the generation of ROS and its degradation capacity in mitochondria may be critical for the determination of lifespan (38), which favors the free radical theory of aging (39, 40). Kops *et al.* (21) recently demonstrated *in vitro* that FOXO3a, a homologue of DAF-16, actually induced the expression of MnSOD, enhancing the antioxidative defense system in cultured mammalian cells challenged with oxidative stress. In the present study we demonstrated for the first time that MnSOD expression is up-regulated *in vivo* by defective insulin signaling in IR mutant mice. Because IR mutant mice carry a mutation homologous with *daf-2* with respect to the severely suppressed signaling of insulin, the up-regulation of MnSOD suggests that one of the longevity signals is sent to the anti-oxidative defense system, which is well conserved between invertebrates and mammals. Although further analyses are needed for elucidation of the molecular basis for the regulation of MnSOD, we found the transcriptional up-regulation of the MnSOD gene in IR mutant mice, suggesting the direct involvement of DAF-16 in the regulation of the mammalian MnSOD gene.

Estrogen Confers Resistance to Oxidative Stress by Up-regulating the MnSOD Gene—As shown in Fig. 4, the acquired

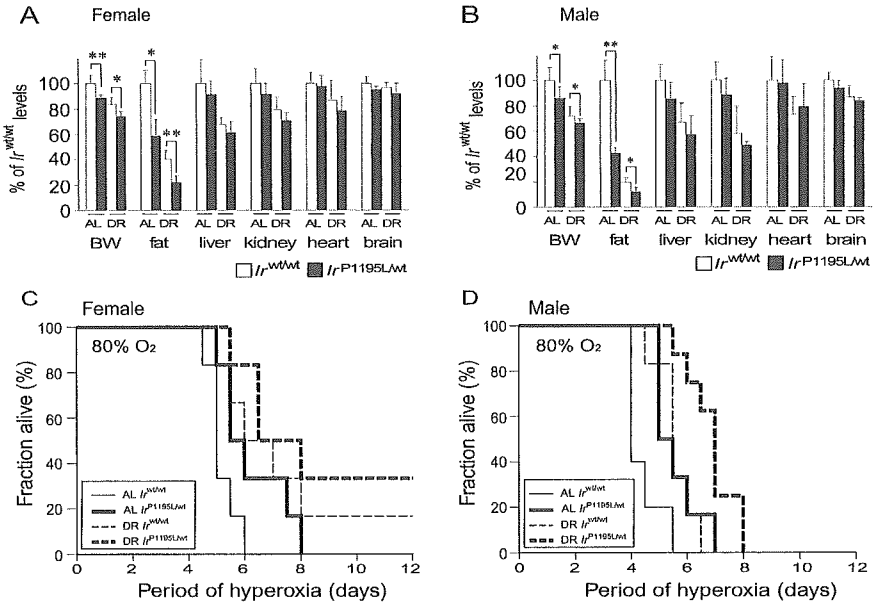

FIG. 7. **The influence of DR in IR mutant mice.** *A* and *B*, comparison of mean body weights (*BW*) and organ weights between $Ir^{P1195L/wt}$ mice and $Ir^{wt/wt}$ mice. $Ir^{P1195L/wt}$ mice had significantly lower body weights than $Ir^{wt/wt}$ mice. The reduction in fat mainly causes the reduction in body weight. *C* and *D*, R additively enhances the resistance against hyperoxygen in $Ir^{P1195L/wt}$ mice. Each *bar* represents the mean ± S.D. in each group from at least five mice per genotype. *, $p < 0.05$; **, $p < 0.01$; $Ir^{P1195L/wt}$ mice *versus* $Ir^{wt/wt}$ mice.

resistance to oxidative stress observed in female IR mutant mice was significantly attenuated when their ovaries were surgically removed. Because the ovary secretes the sex hormones estrogen and progesterone, either or both sex hormones confer resistance to oxidative stress in the mutant mice. To address this endocrinological issue, we administered E2 to male IR mutant mice as well as wild-type littermates. Interestingly, both the mutant and wild-type mice survived longer when they were administered E2, suggesting that estrogen made the male mice resistant to oxidative stress. This result is particularly interesting given that patients with prostate cancer are often prescribed with estradiol for hormone therapy. It is also interesting that female animals including humans generally live longer than males. In this context female hormones may protect the body from oxidative stress during the reproductive period, but the beneficial effects would fade after menopause. These assumptions are highly compatible with the notion that age-associated disease, such as atherosclerosis, osteoporosis, and dementia tend to appear more frequently after menopause in elderly females.

As for the molecular mechanism by which estrogen affects the signaling pathway triggered by insulin, Bailey *et al.* (41) showed that ovariectomized rodents showed an impaired glucose tolerance with an impaired secretion of insulin, suggesting that sex hormones have a direct pharmacological effect on the endocrinological function of insulin. In humans as well, postmenopausal women develop insulin resistance associated with an increase in body fat. Estrogen hormone replacement therapy improves insulin sensitivity with significant loss of fat tissue (42). Because the pharmacological actions of estrogen depend on the receptor subtypes expressed in each tissue, subtype-specific effects of estrogen should be investigated in subtype-specific estrogen receptor (ER)-deficient mice, ERα-deficient or ERβ-deficient mice (43, 44).

DR Confers Distinct Signaling for the Determination of Lifespan—Evidence has accumulated that DR extends the lifespan of animals associated with an enhanced resistance to oxidative stress in various species (28–30). Mutant mice with growth hormone signaling such as Ames dwarf mice showed extended lifespan compared with wild-type mice when they were raised in an ordinary laboratory environment (45–47). Interestingly, these mutant mice had an even longer lifespan when raised with a reduced diet (48). The result suggests that the longevity signaling evoked by DR may be in large part independent and distinct from the insulin signaling, although DR itself suppresses glucose metabolism and insulin secretion because of the restricted dietary intake.

Another genetic model, the fat-specific insulin receptor knock-out mouse, which has a tissue-specific defect of insulin signaling in adipose tissue, showed reduced adiposity without a restriction of diet. These mice also showed extended lifespan even when they were raised with an ordinary diet, suggesting that the reduction in fat mass attributed to the longer lifespan (32). It is, thus, speculated that the amount of fat mass may be a major determinant of lifespan irrespective of environmental factors or genetic factors. In the present study, however, we revealed that the amount of fat mass and the resistance to oxidative stress are not necessarily correlated (Fig. 7, *B* and *D*), suggesting that not only the reduction of fat mass but other environmental or genetic factors contribute to the acquired resistance to oxidative stress. The idea that DR has an independent and distinct signaling mechanism from insulin is also supported by the report that *daf-2* mutants showed additional extension of lifespan in *C. elegans* when their diet of was restricted (33).

In the present study we demonstrated that in IR mutant mice resistance to oxidative stress was further enhanced by DR or E2. We are still finishing an analysis of the lifespan of IR mutant mice under normoxic conditions. We also expect a gender difference in the lifespan of IR mutant mice based on the analysis in oxygen chambers. Female mutant mice may have an enhanced defense system due to the estrogen secreted by the ovaries during the reproductive period. We demonstrated here that three distinct signals, insulin, estrogen, and dietary signals, work in different and independent ways and together increase resistance to oxidative stress and MnSOD levels in mice.

Acknowledgements—We thank Drs. Nakajima, Takahashi, Uchiyama, Moriizumi, Ikegami, Nakai, Huang, Nojiri, Kawakami, Kuwahara, and Sakuramoto for technical assistance. We especially thank Dr. Miyazaki of Osaka University for CAG-Cre transgenic mice, Dr. Ebina of Tokushima University for anti-IR antibody, and Drs. Kojima and Takahashi of Tokyo University of Science for valuable discussions.

REFERENCES

1. Finkel, T., and Holbrook, N. J. (2000) *Nature* **408,** 239–247
2. Martin, G. M., Austad, S. N., and Johnson, T. E. (1996) *Nat. Genet.* **13,** 25–34
3. Kimura, K. D., Tissenbaum, H. A., Liu, Y., and Ruvkun, G. (1997) *Science* **277,** 942–946

4. Kenyon, C., Chang, J., Gensch, E., Rudner, A., and Tabtiang, R. (1993) *Nature* **366,** 461–464
5. Honda, Y., and Honda, S. (1999) *FASEB J.* **13,** 1385–1393
6. Clancy, D. J., Gems, D., Harshman, L. G., Oldham, S., Stocker, H., Hafen, E., Leevers, S. J., and Partridge, L. (2001) *Science* **292,** 104–106
7. Holzenberger, M., Dupont, J., Ducos, B., Leneuve, P., Geloen, A., Even, P. C., Cervera, P., and Le Bouc, Y. (2003) *Nature* **421,** 182–187
8. Smith, D. W. (1989) *Biol. Rev. Camb. Philos. Soc.* **64,** 1–12
9. Borras, C., Sastre, J., Garcia-Sala, D., Lloret, A., Pallardo, F. V., and Vina, J. (2003) *Free Radic. Biol. Med.* **34,** 546–552
10. Ho, Y. S., Vincent, R., Dey, M. S., Slot, J. W., and Crapo, J. D. (1998) *Am. J. Respir. Cell Mol. Biol.* **18,** 538–547
11. Wispe, J. R., Warner, B. B., Clark, J. C., Dey, C. R., Neuman, J., Glasser, S. W., Crapo, J. D., Chang, L. Y., and Whitsett, J. A. (1992) *J. Biol. Chem.* **267,** 23937–23941
12. Taniguchi, M., Sanbo, M., Watanabe, S., Naruse, I., Mishina, M., and Yagi, T. (1998) *Nucleic Acids Res.* **26,** 679–680
13. Nagy, Z. P., Joris, H., Liu, J., Staessen, C., Devroey, P., and Van Steirteghem, A. C. (1993) *Hum. Reprod.* **8,** 2180–2184
14. Sakai, K., and Miyazaki, J. (1997) *Biochem. Biophys. Res. Commun.* **237,** 318–324
15. Imanaka, T., Hayashi, H., Kishi, K., Wang, L., Ishii, K., Hazeki, O., Katada, T., and Ebina, Y. (1998) *J. Biol. Chem.* **273,** 25347–25355
16. Um, S. H., Frigerio, F., Watanabe, M., Picard, F., Joaquin, M., Sticker, M., Fumagalli, S., Allegrini, P. R., Kozma, S. C., Auwerx, J., and Thomas, G. (2004) *Nature* **431,** 200–205
17. Ikegami, T., Suzuki, Y., Shimizu, T., Isono, K., Koseki, H., and Shirasawa, T. (2002) *Biochem. Biophys. Res. Commun.* **296,** 729–736
18. Accili, D., Drago, J., Lee, E. J., Johnson, M. D., Cool, M. H., Salvatore, P., Asico, L. D., Jose, P. A., Taylor, S. I., and Westphal, H. (1996) *Nat. Genet.* **12,** 106–109
19. Joshi, R. L., Lamothe, B., Cordonnier, N., Mesbah, K., Monthioux, E., Jami, J., and Bucchini, D. (1996) *EMBO J.* **15,** 1542–1547
20. Tatar, M., Kopelman, A., Epstein, D., Tu, M. P., Yin, C. M., and Garofalo, R. S. (2001) *Science* **292,** 107–110
21. Kops, G. J., Dansen, T. B., Polderman, P. E., Saarloos, I., Wirtz, K. W., Coffer, P. J., Huang, T. T., Bos, J. L., Medema, R. H., and Burgering, B. M. (2002) *Nature* **419,** 316–321
22. Parkes, T. L., Elia, A. J., Dickinson, D., Hilliker, A. J., Phillips, J. P., and Boulianne, G. L. (1998) *Nat. Genet.* **19,** 171–174
23. Phillips, J. P., Parkes, T. L., and Hilliker, A. J. (2000) *Exp. Gerontol.* **35,** 1157–1164
24. Strehlow, K., Rotter, S., Wassmann, S., Adam, O., Grohe, C., Laufs, K., Bohm, M., and Nickenig, G. (2003) *Circ. Res.* **93,** 170–177
25. Kitamura, T., Kahn, C. R., and Accili, D. (2003) *Annu. Rev. Physiol.* **65,** 313–332
26. Pedersen, S. B., Borglum, J. D., Moller-Pedersen, T., and Richelsen, B. (1992) *Mol. Cell. Endocrinol.* **85,** 13–19
27. Yu, X., Rajala, R. V., McGinnis, J. F., Li, F., Anderson, R. E., Yan, X., Li, S., Elias, R. V., Knapp, R. R., Zhou, X., and Cao, W. (2004) *J. Biol. Chem.* **279,** 13086–13094
28. Hamilton, M. L., Van Remmen, H., Drake, J. A., Yang, H., Guo, Z. M., Kewitt, K., Walter, C. A., and Richardson, A. (2001) *Proc. Natl. Acad. Sci. U. S. A.* **98,** 10469–10474
29. Lee, S. S., and Ruvkun, G. (2002) *Nature* **418,** 287–288
30. Sohal, R. S., and Weindruch, R. (1996) *Science* **273,** 59–63
31. Bluher, M., Michael, M. D., Peroni, O. D., Ueki, K., Carter, N., Kahn, B. B., and Kahn, C. R. (2002) *Dev. Cell* **3,** 25–38
32. Bluher, M., Kahn, B. B., and Kahn, C. R. (2003) *Science* **299,** 572–574
33. Houthoofd, K., Braeckman, B. P., Johnson, T. E., and Vanfleteren, J. R. (2003) *Exp. Gerontol.* **38,** 947–954
34. Lin, K., Dorman, J. B., Rodan, A., and Kenyon, C. (1997) *Science* **278,** 1319–1322
35. Ogg, S., Paradis, S., Gottlieb, S., Patterson, G. I., Lee, L., Tissenbaum, H. A., and Ruvkun, G. (1997) *Nature* **389,** 994–999
36. Giannakou, M. E., Goss, M., Junger, M. A., Hafen, E., Leevers, S. J., and Partridge, L. (2004) *Science* **305,** 361
37. Furuyama, T., Nakazawa, T., Nakano, I., and Mori, N. (2000) *Biochem. J.* **349,** 629–634
38. Ku, H. H., Brunk, U. T., and Sohal, R. S. (1993) *Free Radic. Biol. Med.* **15,** 621–627
39. Harman, D. (1956) *J. Gerontol.* **11,** 298–300
40. Beckman, K. B., and Ames, B. N. (1998) *Physiol. Rev.* **78,** 547–581
41. Bailey, C. J., and Ahmed-Sorour, H. (1980) *Diabetologia* **19,** 475–481
42. Tchernof, A., Calles-Escandon, J., Sites, C. K., and Poehlman, E. T. (1998) *Coron. Artery Dis.* **9,** 503–511
43. Heine, P. A., Taylor, J. A., Iwamoto, G. A., Lubahn, D. B., and Cooke, P. S. (2000) *Proc. Natl. Acad. Sci. U. S. A.* **97,** 12729–12734
44. Krege, J. H., Hodgin, J. B., Couse, J. F., Enmark, E., Warner, M., Mahler, J. F., Sar, M., Korach, K. S., Gustafsson, J. A., and Smithies, O. (1998) *Proc. Natl. Acad. Sci. U. S. A.* **95,** 15677–15682
45. Flurkey, K., Papaconstantinou, J., Miller, R. A., and Harrison, D. E. (2001) *Proc. Natl. Acad. Sci. U. S. A.* **98,** 6736–6741
46. Brown-Borg, H. M., Borg, K. E., Meliska, C. J., and Bartke, A. (1996) *Nature* **384,** 33
47. Bartke, A. (2000) *Results Probl. Cell Differ.* **29,** 181–202
48. Bartke, A., Wright, J. C., Mattison, J. A., Ingram, D. K., Miller, R. A., and Roth, G. S. (2001) *Nature* **414,** 412

nature medicine

Angiopoietin-related growth factor antagonizes obesity and insulin resistance

Yuichi Oike[1], Masaki Akao[1], Kunio Yasunaga[2], Toshimasa Yamauchi[3], Tohru Morisada[1], Yasuhiro Ito[1], Takashi Urano[1], Yoshishige Kimura[1], Yoshiaki Kubota[1], Hiromitsu Maekawa[1], Takeshi Miyamoto[1], Keishi Miyata[1], Shun-ichiro Matsumoto[2], Juro Sakai[4], Naomi Nakagata[5], Motohiro Takeya[6], Haruhiko Koseki[7], Yoshihiro Ogawa[8], Takashi Kadowaki[3] & Toshio Suda[1]

Angiopoietin-related growth factor (AGF), a member of the angiopoietin-like protein (Angptl) family, is secreted predominantly from the liver into the systemic circulation. Here, we show that most (>80%) of the AGF-deficient mice die at about embryonic day 13, whereas the surviving AGF-deficient mice develop marked obesity, lipid accumulation in skeletal muscle and liver, and insulin resistance accompanied by reduced energy expenditure relative to controls. In parallel, mice with targeted activation of AGF show leanness and increased insulin sensitivity resulting from increased energy expenditure. They are also protected from high-fat diet–induced obesity, insulin resistance and nonadipose tissue steatosis. Hepatic overexpression of AGF by adenoviral transduction, which leads to an approximately 2.5-fold increase in serum AGF concentrations, results in a significant ($P < 0.01$) body weight loss and increases insulin sensitivity in mice fed a high-fat diet. This study establishes AGF as a new hepatocyte-derived circulating factor that counteracts obesity and related insulin resistance.

© 2005 Nature Publishing Group http://www.nature.com/naturemedicine

Obesity is an increasingly prevalent medical and social problem with potentially devastating consequences because it clusters with type 2 diabetes, hypertension and hyperlipidemia in the metabolic syndrome or syndrome X[1,2]. The molecular mechanisms underlying obesity have not been fully clarified, and effective therapeutic approaches are currently of general interest. Inhibition of weight gain requires that we burn more calories than we take in. From this perspective, adaptive thermogenesis, which is the process of heat production in response to diet or environment temperature, is an important defense against obesity[3,4].

Recently, we and several groups independently identified several molecules containing a coiled-coil domain and a fibrinogen-like domain, motifs structurally conserved in angiopoietins[5,6]. Because these molecules do not bind the angiopoietin receptor, Tie-2, they were named angiopoietin-like proteins (Angptl). We identified angiopoietin-related growth factor (AGF, also known as Angptl6 and encoded by the gene *Angptl6*) as a member of the Angptl family and showed that it is a circulating orphan peptide secreted by liver that induces angiogenesis and proliferation of skin cells, and thereby promotes wound healing[6–8]. Furthermore, several early reports have indicated that there are additional members of the Angptl family, which are currently considered orphan ligands, as angiogenic factors in the vascular system[6,9–11]. On the other hand, several reports indicate that Angptls have biological effects on nonvascular cells. For example, Angptl4 (refs. 12,13; also known as PGAR and FIAF) and Angptl3 (refs. 14,15) regulate fat and/or lipid metabolic homeostasis in addition to controlling angiogenesis[10,11]. These findings suggest that Angptls exert multiple biological functions; however, the physiological and pathological roles of each member of the Angptls have not been fully clarified.

Here we show that most (>80%) of the mice with mutations in AGF (*Angptl6*$^{-/-}$ mice) die at about embryonic day 13, with apparent cardiovascular defects including poorly formed yolk sac and vitelline vessels. Notably, the surviving *Angptl6*$^{-/-}$ mice become markedly obese and have obesity-related metabolic disorders. In parallel, mice with targeted activation of AGF *in vivo* (*Angptl6*-transgenic mice) show markedly reduced adiposity and insulin sensitivity. Furthermore, *Angptl6*-transgenic mice are completely resistant to high-fat diet–induced obesity and impaired insulin sensitivity. Moreover, we found that hepatic overexpression of AGF by adenoviral transduction, which leads to an approximately 2.5-fold increase in serum AGF concentrations, results in a significant ($P < 0.01$) body weight loss and ameliorates insulin sensitivity in mice fed a high-fat diet. Based on these findings, we report here that AGF is a new hepatocyte-derived circulating factor counteracting high-fat diet–induced obesity and related insulin resistance through increased energy expenditure, thereby suggesting a therapeutic potential in counteracting obesity and diabetes.

[1]Department of Cell Differentiation, The Sakaguchi Laboratory, School of Medicine, Keio University, 35 Shinanomachi, Shinjuku-ku, Tokyo 160-8582, Japan. [2]Molecular Medicine Laboratories, Yamanouchi Pharmaceutical Co., Ltd., Tsukuba, 305-8585, Japan. [3]Department of Internal Medicine, Graduate School of Medicine, University of Tokyo, Tokyo 113-8655, Japan. [4]Research Center for Advanced Science and Technology, University of Tokyo, Tokyo 153-8904, Japan. [5]Center for Animal Resources and Development, and [6]Department of Pathology, Kumamoto University, Kumamoto 860-0811, Japan. [7]RIKEN Research Center for Allergy and Immunology, Tsurumi-ku, Yokohama 230-0045, Japan. [8]Department of Molecular Medicine and Metabolism, Medical Research Institute, Tokyo Medical and Dental University, Tokyo 101-0062, Japan. Correspondence should be addressed to Y.O. (oike@sc.itc.keio.ac.jp).

Published online 20 March 2005; doi:10.1038/nm1214

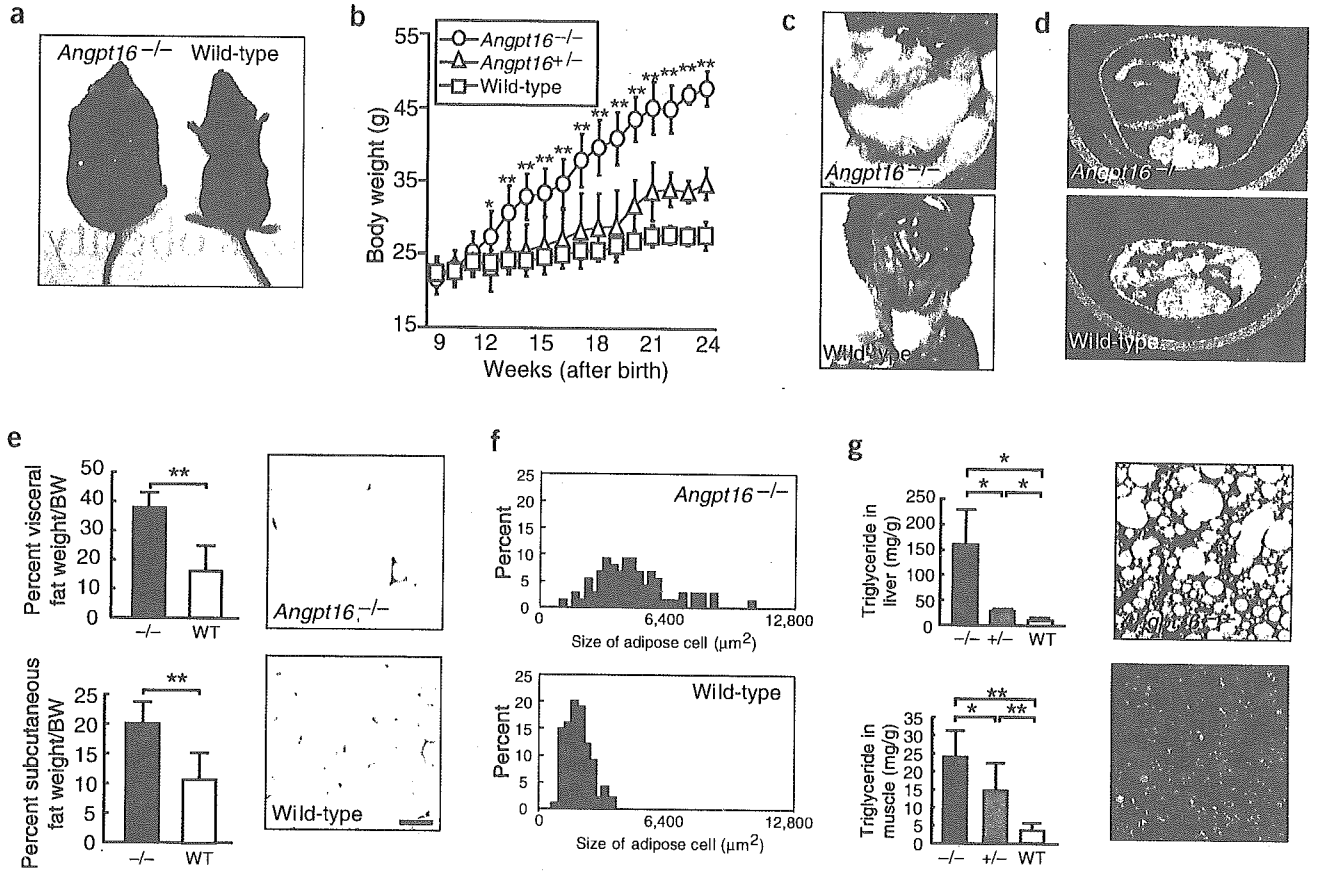

Figure 1 Obesity in *Angptl6*$^{-/-}$ mice on a normal diet. (**a**) Gross appearance of *Angptl6*$^{-/-}$ mice and wild-type control mice. (**b**) Body weight of each genotype ($n = 8$). (**c–g**) Abdominal cavity (**c**), CT findings at a level of 8 mm above the top of the iliac bone (**d**), visceral fat ($n = 5$) and subcutaneous fat ($n = 5$) weight/body weight, and histological analysis (**e**) and distribution of cell size (**f**) of WAT of *Angptl6*$^{-/-}$ mice and wild-type mice. (**g**) Triglyceride levels in liver ($n = 5$) and gastrocnemius muscle ($n = 5$), and hematoxylin and eosin–stained sections of BAT of *Angptl6*$^{-/-}$ and wild-type mice. Data are mean ± s.d. Bars in histological sections indicate 50 μm. $^{*}P < 0.05$, $^{**}P < 0.01$, between the two genotypes indicated. Female mice 8 months after birth were used for all experiments.

© 2005 Nature Publishing Group http://www.nature.com/naturemedicine

RESULTS

Disruption of *Angptl6 in vivo*

To investigate the physiological role of AGF, we generated mice with mutations in *Angptl6* (**Supplementary Fig. 1** online). Most (>80%) of *Angptl6*$^{-/-}$ mice die at approximately embryonic day 13 (**Supplementary Fig. 1**), with apparent cardiovascular defects including poorly formed yolk sac and vitelline vessels (data not shown). Notably, the surviving *Angptl6*$^{-/-}$ mice become markedly obese even on a normal chow diet, suggesting that AGF has a crucial role in regulating adiposity in adulthood (**Fig. 1a**). We therefore focused on how AGF functions in the pathogenesis of obesity and associated disorders.

Obesity in *Angptl6*$^{-/-}$ mice

Twelve weeks after birth, *Angptl6*$^{-/-}$ mice showed increases in body weight that surpassed those seen in wild-type (*Angptl6*$^{+/+}$) mice on a normal chow diet (**Fig. 1b**). There were no phenotypic differences between male and female mice. Macroscopic and computed tomographic (CT) analyses taken 8 months after birth showed that both visceral and subcutaneous fat depots were significantly increased in *Angptl6*$^{-/-}$ mice compared to wild-type mice (**Fig. 1c–e**). Sections of white adipose tissue (WAT) from *Angptl6*$^{-/-}$ mice showed increased adipocyte size relative to controls (**Fig. 1e,f**). A large amount of lipid accumulation in liver, skeletal muscle and brown adipose tissue (BAT) was observed in *Angptl6*$^{-/-}$ mice compared with *Angptl6*$^{+/-}$ and wild-type mice (**Fig. 1g**).

Metabolic disorders in *Angptl6*$^{-/-}$ mice

To address alternative causes of increased body weight in *Angptl6*$^{-/-}$ mice, we compared lipid metabolism, rectal temperature, basal metabolic rate and food intake of *Angptl6*$^{-/-}$ and wild-type mice. Significant increases were observed in serum cholesterol and free fatty acid (FFA) concentrations in *Angptl6*$^{-/-}$ mice, whereas there were no significant differences in serum triglyceride concentration between genotypes (**Fig. 2a**). *Angptl6*$^{-/-}$ mice also showed significant decreases in rectal temperature and whole-body oxygen consumption rates compared with wild-type mice (**Fig. 2b**). A small, statistically insignificant increase was observed in daily food intake in *Angptl6*$^{-/-}$ mice compared with controls (**Fig. 2b**).

Adipose tissue has a substantial influence on systemic glucose homeostasis through secretion of adipocytokines[2,16,17]. *Angptl6*$^{-/-}$ mice showed mild hyperglycemia and severe hyperinsulinemia (**Fig. 2c**). To investigate this point further, we performed intraperitoneal glucose and insulin tolerance tests (IGTT and IITT, respectively). Both hyperglycemia and hyperinsulinemia were detected in *Angptl6*$^{-/-}$ mice throughout the time course of the experiment

(Fig. 2c). Moreover, the glucose-lowering effect of insulin was decreased in *Angptl6*$^{-/-}$ mice relative to controls, indicating insulin resistance in *Angptl6*$^{-/-}$ mice (Fig. 2d). Recent studies have shown a role for tumor necrosis factor (TNF)-α[18,19] secreted from adipose tissue as a mediator of insulin resistance, and adiponectin[20,21] and leptin[22,23] have a role in insulin sensitivity. The leptin concentration in *Angptl6*$^{-/-}$ mice was significantly higher than that seen in controls, whereas no significant differences were observed in adiponectin and TNF-α concentrations between genotypes (Fig. 2e).

Molecular alterations in *Angptl6*$^{-/-}$ mice

The physiological data presented above indicate that inactivation of AGF *in vivo* leads to decreased energy expenditure and obesity. Recent studies indicate that BAT and skeletal muscle function as tissues mediating adaptive thermogenesis, which is an important defense against obesity[24,25]. To determine the molecular basis of these metabolic changes in *Angptl6*$^{-/-}$ mice, we examined the expression of molecules with proposed roles in obesity and associated metabolic action in BAT and skeletal muscle. Quantitative RT-PCR analysis showed significant decreases in expression of PPARα, PPARγ, PGC-1β and UCP1 in BAT (Fig. 2f) and PPARδ and UCP3 in skeletal muscle (Fig. 2g) in *Angptl6*$^{-/-}$ mice, suggesting that such alterations in gene expression underlie susceptibility to obesity in *Angptl6*$^{-/-}$ mice.

Generation of *Angptl6*-transgenic mice

Observations that AGF ablation causes obesity prompted us to further investigate whether AGF functions in resistance to obesity and associated disorders. To generate mice overexpressing AGF constitutively, we targeted the activation of *Angptl6 in vivo* by driving its expression from the chicken β-actin promoter with the cytomegalovirus immediate-early enhancer (CAG promoter)[26,27] (**Supplementary Fig. 2** online). The CAG promoter has been reported to be strongly active in a variety of tissues. In our mice, the promoter drove high expression of the *Angptl6* transgene in BAT, heart and skeletal muscle relative to expression of the endogenous gene in each tissue (**Supplementary Fig. 2**). AGF concentration in the circulation of *Angptl6* transgenic mice increased approximately twofold compared with basal concentrations in nontransgenic controls (Fig. 3a).

Leanness in *Angptl6* transgenic mice

Despite a daily food intake similar to that of controls when individually housed and fed a normal chow diet (transgenic mice, 0.17 ± 0.05

© 2005 Nature Publishing Group http://www.nature.com/naturemedicine

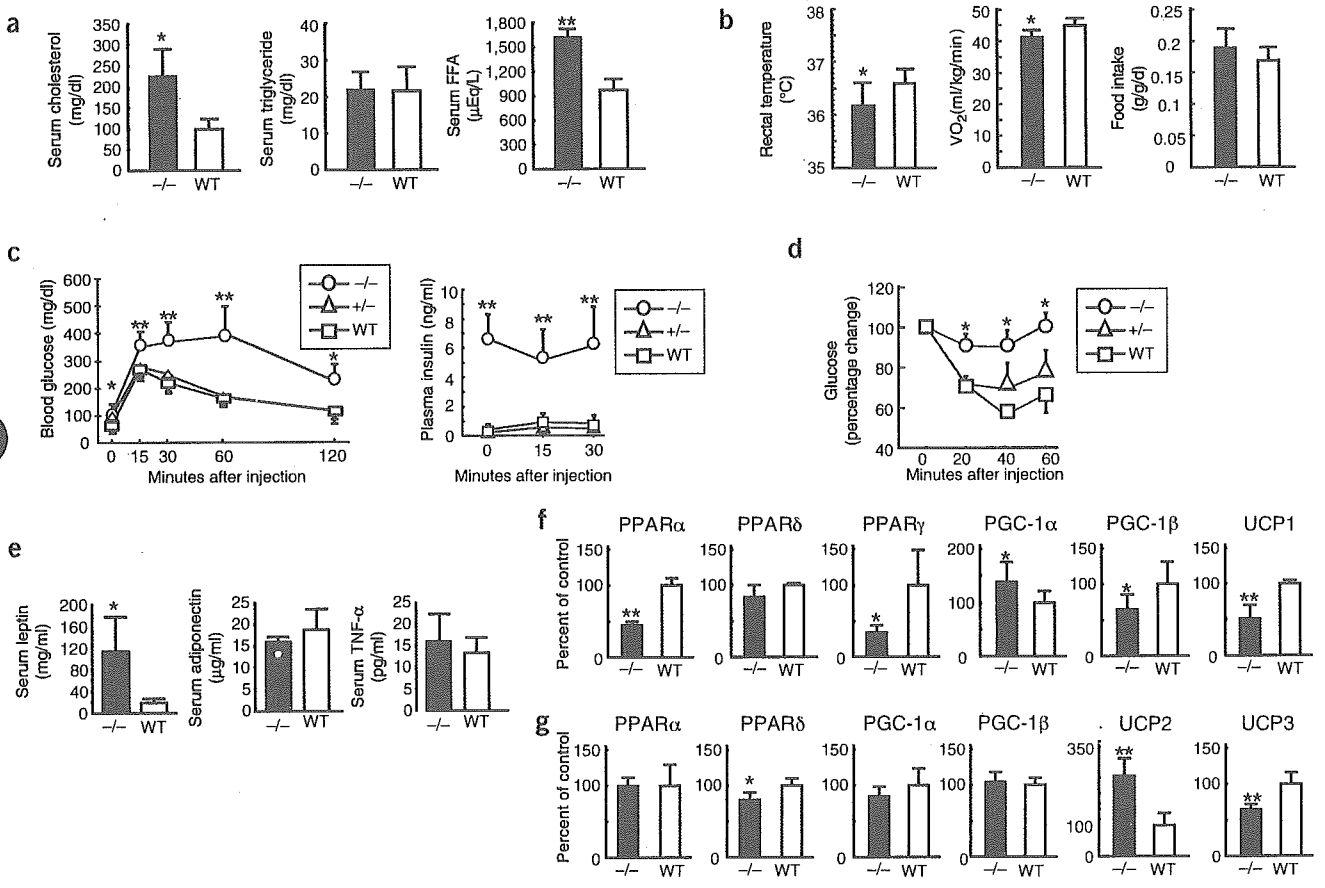

Figure 2 Metabolic effects of AGF deficiency on a normal diet. (**a**) Serum cholesterol, triglyceride and FFA concentrations in *Angptl6*$^{-/-}$ and wild-type control mice at 5 months of age ($n = 5$ in each group). (**b**) Rectal temperature, oxygen consumption (VO_2)/lean body weight and food intake/lean body weight in *Angptl6*$^{-/-}$ and wild-type mice at 6 months of age ($n = 8$ in each group). (**c**,**d**) Glucose (**c**) and insulin (**d**) tolerance tests in *Angptl6*$^{-/-}$, *Angptl6*$^{+/-}$ and wild-type mice at 3 months of age ($n = 6$ in each group). (**e**) Serum leptin, adiponectin, and TNF-α concentrations in *Angptl6*$^{-/-}$ and wild-type mice at 5 months of age ($n = 5$ in each group). (**f**,**g**) Expression of genes associated with energy expenditure in BAT (**f**) and skeletal muscle (**g**) of *Angptl6*$^{-/-}$ relative to wild-type mice (100%) at 3 months of age ($n = 5$ in each group). Data are mean ± s.d. $^*P < 0.05$, $^{**}P < 0.01$, between the two genotypes indicated or among three genotypes. Female mice were used for all experiments.

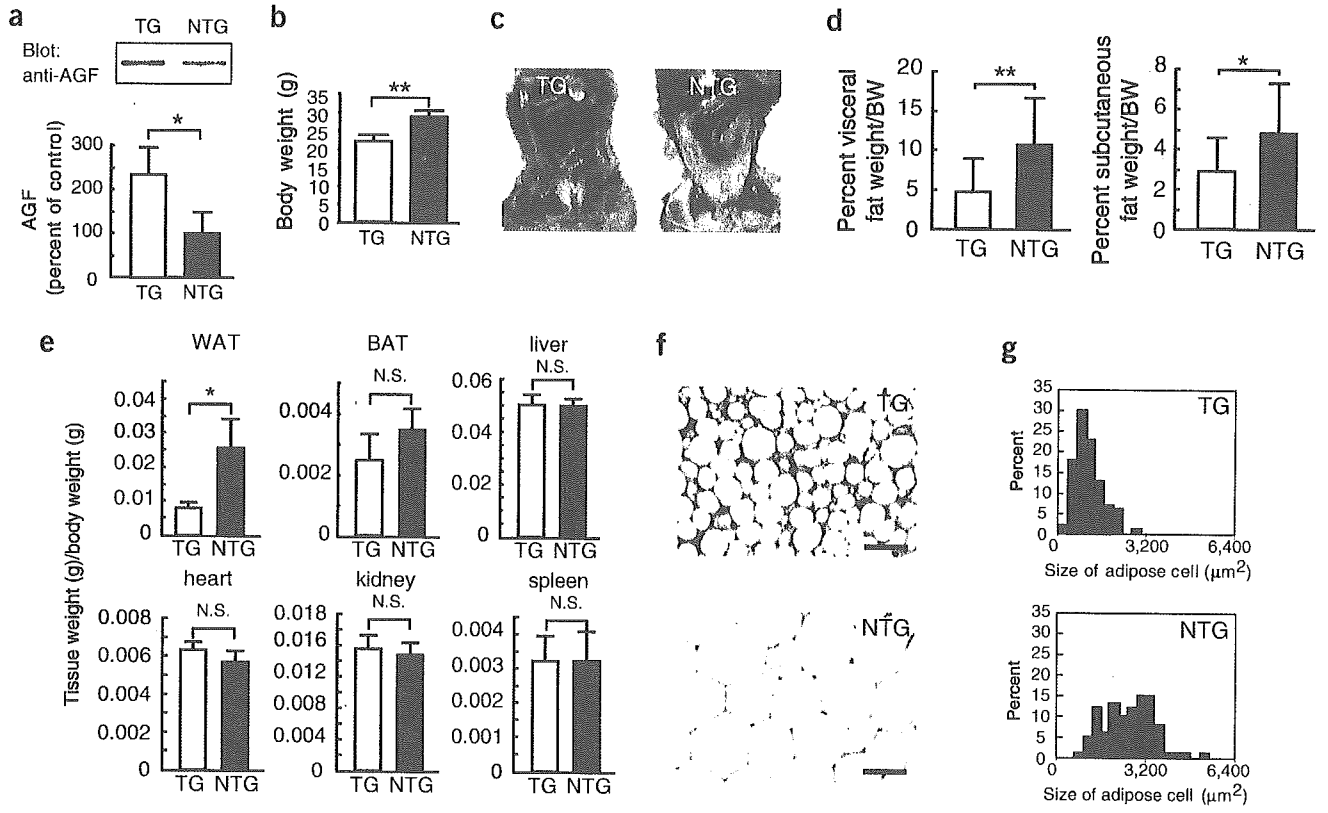

Figure 3 *Angptl6* transgenic mice are lean as a result of a loss of WAT mass. (**a**) Western blotting analysis for serum AGF in *Angptl6* transgenic (TG) and nontransgenic control (NTG) mice at 4 months of age. The ratio for the control is set as 100%. (**b–g**) Body weight (**b**), and gross appearance of visceral adipocyte (**c**) in TG and NTG mice at 4 months of age. (**d**) Comparison of visceral fat and subcutaneous fat weight/body weight between TG and NTG mice at 5 months of age. Tissue weight/body weight in TG and NTG mice at 4 months of age (**e**). $n = 10–15$ in each group. Histological analysis (**f**) and distribution of cell size (**g**) of WAT from TG and NTG mice at 4 months of age. Scale bars, 50 μm. Data are mean ± s.d. $^*P < 0.05$, $^{**}P < 0.01$, between the two genotypes indicated. N.S. indicates no significant difference compared with nontransgenic wild-type mice. Female mice were used for all experiments.

© 2005 Nature Publishing Group http://www.nature.com/naturemedicine

versus control mice, 0.15 ± 0.03 g/g lean body mass/d), 5-month-old *Angptl6* transgenic mice showed marked reductions in body weight and adiposity compared with controls (**Fig. 3b–d**). Although there was no alteration in body weight at birth between genotypes, a reduction in body weight of *Angptl6* transgenic mice compared to controls was noted 4 weeks after birth and persisted throughout their life. There were no differences of this alteration in body weight between male and female mice. Furthermore, only WAT weight per body weight in *Angptl6* transgenic mice was markedly decreased compared to that of controls (**Fig. 3e**). Adipocytes from *Angptl6* transgenic mice are smaller in size compared to those from controls, indicating that a reduction in total fat mass may result from decreased triglyceride accumulation (**Fig. 3f,g**).

Metabolic alterations in *Angptl6* transgenic mice

There was no difference in *in vitro* adipocyte differentiation of embryonic fibroblasts between *Angptl6* transgenic mice and controls (data not shown). To address alternative causes for decreased adiposity in *Angptl6* transgenic mice, we compared rectal temperature and basal metabolic rates of *Angptl6* transgenic mice and controls. Transgenic mice showed a small, statistically insignificant increase in rectal temperature and a statistically significant increase in whole-body oxygen consumption rates relative to controls (**Fig. 4a**), suggesting the enhanced energy expenditure in *Angptl6* transgenic mice. The microvasculature assists in heat dissipation at sites of active thermogenesis, increasing the efficiency of lipid release from fat stores[28,29]. *Angptl6* transgenic mice showed an increase in the number of capillary-sized vessels in skeletal muscles compared to controls (**Fig. 4b**), suggesting that AGF assists in part to increase thermogenesis in *Angptl6* transgenic mice.

Quantitative RT-PCR analysis showed significant increases in expression of the genes encoding PPARα, PPARγ and PGC-1β in BAT (**Fig. 4c**) and of the genes encoding PPARα, PPARδ, PGC-1α and UCP2 in skeletal muscle (**Fig. 4d**) in *Angptl6* transgenic mice. These findings suggest that overexpression of AGF *in vivo* activates molecules involved in stimulating energy expenditure, and thereby leads to decreased adiposity.

Insulin sensitivity in *Angptl6* transgenic mice

A lack of fat causes decreases in serum levels of leptin and adiponectin and leads to insulin resistance and diabetes[21,22,30,31]. Although *Angptl6* transgenic mice showed decreased serum leptin levels, identical serum adiponectin levels were observed in transgenic and wild-type mice (**Fig. 4e**). Serum adiponectin levels per WAT mass in *Angptl6* transgenic mice were markedly increased compared with that of wild-type mice, whereas there was no difference in serum leptin levels per WAT mass (**Fig. 4e**), suggesting that adipose tissues in *Angptl6* transgenic mice secrete adiponectin abundantly. Notably, IGTT and IITT showed that *Angptl6* transgenic mice show increased insulin sensitivity despite the greatly decreased serum leptin and identical serum adiponectin levels